

Robust Control of a Disk Drive Servo System ¹

P.Hr. Petkov², D.-W. Gu³ and M.M. Konstantinov⁴

December 2001

¹This document presents research results of the European Community BRITE-EURAM III Thematic Networks Programme NICONET (contract number BRRT-CT97-5040) and is distributed by the Working Group on Software WGS. *WGS secretariat*: Mrs. Ida Tassens, ESAT - Katholieke Universiteit Leuven, Kasteelpark Arenberg 10, 3001-Leuven-Heverlee, BELGIUM. This report is also available by anonymous ftp from [wgs.esat.kuleuven.ac.be/pub/WGS/REPORTS/SLWN2001-7.ps.Z](ftp://wgs.esat.kuleuven.ac.be/pub/WGS/REPORTS/SLWN2001-7.ps.Z)

²Technical University of Sofia, Department of Automatics, 1756 Sofia, Bulgaria.

³University of Leicester, Department of Engineering, Leicester LE1 7RH, U.K.

⁴University of Architecture & Civil Engineering, 1 Hr. Smirnenski Blv., 1421 Sofia, Bulgaria.

Abstract

In this expository paper we show the application of some of the *SLICOT* routines in the robust control analysis and design of a disk drive servo system. An uncertainty model of the system plant is first derived which contains eleven uncertain parameters including four resonance frequencies, four damping coefficients and three rigid body model parameters. Three controllers for the uncertain system are designed using, respectively, the techniques of \mathcal{H}_∞ mixed sensitivity design, \mathcal{H}_∞ loop shaping design procedure (LSDP) and μ synthesis method. With these controllers the closed-loop system achieves robust stability and in the cases of \mathcal{H}_∞ and μ controllers the closed loop system practically achieves robust performance. A detailed comparison of the frequency domain and time domain characteristics of the closed-loop system with the three controllers is conducted. Further, model reduction routines have been applied to find a reasonably low order controller based on the μ -synthesis design. This reduced order controller maintains the robust stability and robust performance of the closed-loop system. Simulations of the nonlinear sampled-data servo system with the low order controller have been included as well, which confirms the practical applicability of the controller obtained.

Key Words: Robust control systems design, \mathcal{H}_∞ design, Loop Shaping Design, μ -analysis and synthesis, *SLICOT*

Contents

1	Introduction	2
2	Description of the Disk Drive Servo System	2
3	Derivation of the uncertainty model	8
4	Closed-loop system performance requirements	14
5	\mathcal{H}_∞ design	20
6	Loop Shaping Design	24
7	μ-design	29
8	Comparison of the systems with three controllers	36
9	Order reduction of the μ-controller	40
10	Simulation of the nonlinear servo system	42
11	Conclusions	46

1 Introduction

This paper presents an industrial example of robust control systems design using the \mathcal{H}_∞ optimisation, \mathcal{H}_∞ Loop Shaping Design Procedure (LSDP) method and μ -synthesis. The example is a robust design of a disk drive servo system. Major computation steps of all three design methods have been programmed in Fortran 77 and are available in the SLICOT library [1].

In the paper, we show in details how to design a controller for the servo system of a conventional hard disk drive with a single voice-coil-motor (VCM), to ensure robust stability and good nominal and robust performance of the closed-loop system. The routines from SLICOT library are implemented in the form of mex-files which allows to use them easily in MATLAB ¹.

The prevalent trend in hard disk design is towards smaller disks with increasing larger capacities. This implies that the track width has to be smaller leading to lower error tolerance in the positioning of the head. The controller for track following has to achieve tighter regulation in the control of the servomechanism in the presence of parameter variations, nonlinearities and noise. Hence it is appropriate to use advanced design methods like \mathcal{H}_∞ optimisation and μ synthesis to achieve robust stability and robust performance.

2 Description of the Disk Drive Servo System

The schematic diagram of the Disk Drive Servo Control System is shown in Figure 1 and the block-diagram of the system is shown in Figure 2. The read/write (R/W) head is moved by a VCM which is driven by the output current i_c of a power amplifier (PA). The position of the head is measured by a high sensitive sensor. The actual position signal y is compared with the signal y_{ref} which represents the desired head position. y_r is a digital reference for the desired track. The error signal is discretized by an analog-to-digital (A/D) converter and serves as an input to the digital controller K_d which is typically realised on a DSP chip. The output of the controller is converted to analog form by a digital-to-analog converter (D/A) and amplified by the PA. f_d denotes the force disturbance due to external shock and vibrations, power amplifier noise and digital-to-analog converter noise.

The dynamics of an ideal VCM actuator as a rigid body can be represented as a second order state space model in the form

$$\begin{bmatrix} \dot{y} \\ \dot{v}_r \end{bmatrix} = \begin{bmatrix} 0 & k_y \\ 0 & 0 \end{bmatrix} \begin{bmatrix} y \\ v_r \end{bmatrix} + \begin{bmatrix} 0 \\ k_v \end{bmatrix} u$$

¹MATLAB is a trade mark of The Mathworks, Inc.

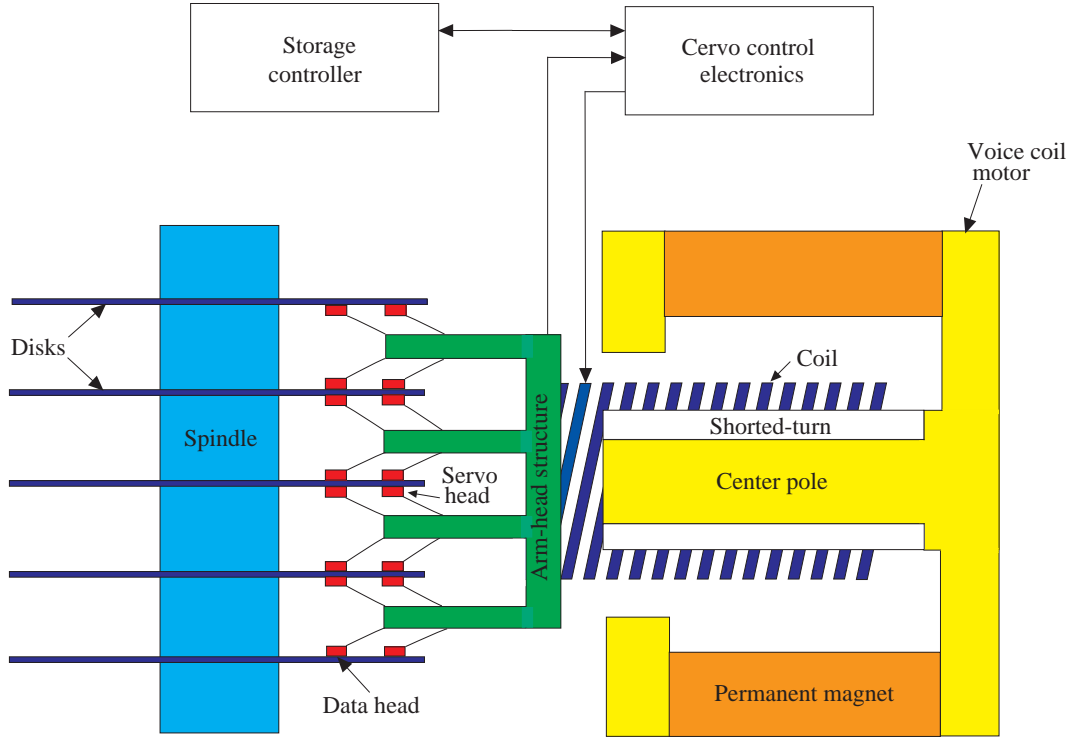


Figure 1: Schematic diagram of the Disk Drive Servo System

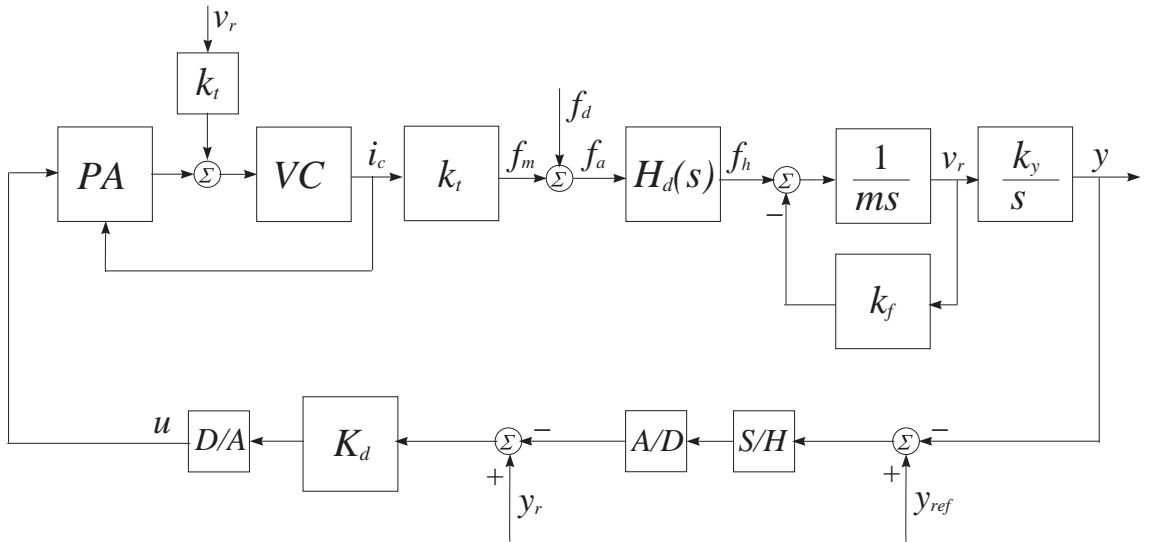


Figure 2: Block diagram of the Disk Drive Servo System

where u is the actuator input (in volts), y and v_r are the position (in tracks) and the velocity of the R/W head, respectively, k_y is the position measurement gain and $k_v = k_t/m$, with k_t being the current/force conversion coefficient and m being the mass of the VCM actuator. Thus the transfer function of the ideal VCM is a double integrator, i.e.

$$G_r(s) = \frac{k_v k_y}{s^2}.$$

In fact, the voice coil has a resistance R_{coil} and inductance L_{coil} , so that the voice coil admittance is

$$\frac{i_c(s)}{e_c(s)} = \frac{1/R_c}{sL_{coil}/R_c + 1},$$

where $R_c = R_{coil} + R_s$, and R_s is the current sense resistance in the power amplifier feedback. Since the corresponding electric time constant L_{coil}/R_c is large, to speedup the coil transient response an additional shortened turn, in the form of a thin layer of gold or low-oxygen content copper plated on the permanent magnet, is used. The transfer function of the voice coil with the shortened turn is

$$\frac{i_c(s)}{e_c(s)} = \frac{1}{R_c} \frac{\tau_z s + 1}{\tau_{p1} \tau_{p2} s^2 + (\tau_{p1} + \tau_z)s + 1},$$

where

$$\begin{aligned} \tau_z &= \frac{L_{coil} + L_{st}}{R_{st}}, \\ \tau_{p1} &= \frac{L_{coil}}{R_c}, \\ \tau_{p2} &= \frac{L_{st}}{R_{st}} \end{aligned}$$

and R_{st} , L_{st} are the resistance and inductance of the shortened turn.

The parameters of the rigid body model are given in Table 1 [2].

The block diagram of the power amplifier with voice coil is shown in Figure 3. The input of the voice coil is the difference $e_p - e_b$, where e_p is the output voltage of the amplifier and $e_b = k_t v_r$ is the back emf which is generated during the moving of the coil in the magnetic field. Since the saturation voltage of the amplifier is e_{\max} , the maximum steady state current in the coil is e_{\max}/R_c . There is a negative current feedback in the amplifier which is realized by the resistance R_s . In the study of the linearized system the back emf and the amplifier saturation are neglected and as a result we obtain the transfer function

$$G_{vca} = \frac{i_c(s)}{u(s)} = \frac{k_{PA}(\tau_z s + 1)}{R_c \tau_{p1} \tau_{p2} s^2 + [R_c \tau_{p1} + (R_c + k_{PA} R_s) \tau_z] s + R_c + K_{PA} R_s}$$

In the given case the amplifier gain k_{PA} is chosen equal to 11, so that the loop gain

$$\frac{k_{PA}}{R_c + K_{PA} R_s}$$

Table 1: Rigid body model parameters and tolerances

Parameter	Description	Value	Units	Tolerance
m	moving mass of the actuator	0.200	kg	$\pm 3.0\%$
k_t	force constant	20.0	N/A	$\pm 10.0\%$
k_y	position measurement gain	10000.0	V/m	$\pm 5.0\%$
R_{coil}	coil resistance	8.00	Ω	$\pm 20.0\%$
R_s	sense resistance in the power amplifier feedback	0.25	Ω	$\pm 1.0\%$
R_{st}	shortened turn resistance	5.00	Ω	$+0, -6\%$
L_{coil}	coil inductance	0.01	H	$+0, -15\%$
L_{st}	shortened turn inductance	0.002	H	$+0, -15\%$
e_{max}	saturated power amplifier voltage	34.0	V	$-0, +5\%$
k_{fric}	viscous friction coefficient	2.51	Ns/m	$\pm 7.5\%$
RPM	disk rotation rate	3623	rev/min	$\pm 3.0\%$
t_w	track width	12.5	μm	$\pm 1.0\%$

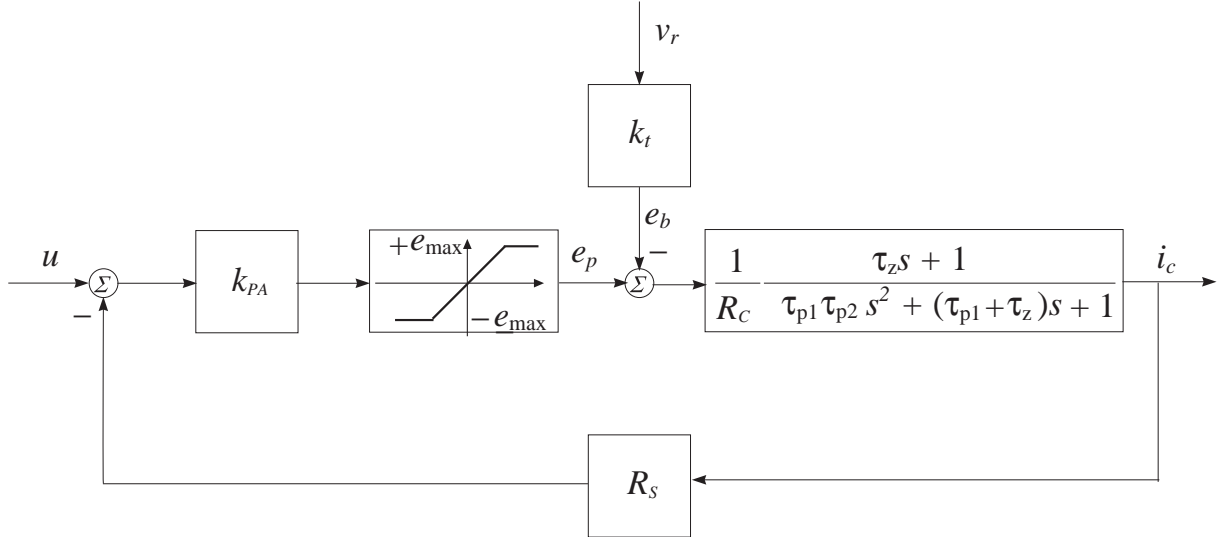


Figure 3: Block diagram of the power amplifier with voice coil

is equal to 1. This means that in the absence of back emf the amplifier will saturate for an input voltage u greater than e_{\max}/R_c (about 4.12 V).

In practice we must also take into account the viscous friction force $k_f v_r$ and the high frequency resonance modes of the head disk assembly represented by the transfer function $H_d(s)$. $H_d(s)$ consists of four flexible (resonance) modes and is obtained as as

$$H_d(s) = \sum_{j=1}^4 \frac{b_{2j}\omega_j s + b_{2j-1}\omega_j^2}{s^2 + 2\xi_j\omega_j s + \omega_j^2}$$

(see Figure 4).

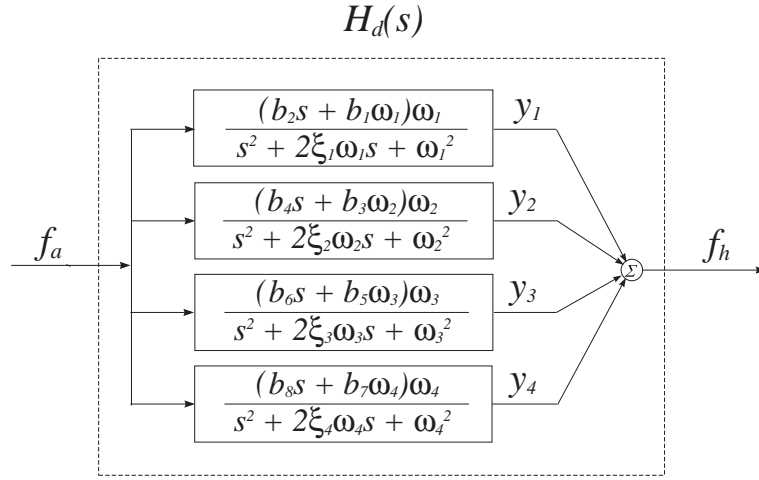


Figure 4: Flexible Modes transfer functions

Here ω_j , ξ_j and b_{2j} , b_{2j-1} are the resonance frequency, the damping coefficient and the coupling coefficients for the j -th mode, for $j=1,\dots,4$. The resonance parameters are determined experimentally and are shown in Table 2 [2].

It is important to note that all model parameters are known with some tolerances and may vary with the changing of working conditions and with the time. Also, the closed-loop system can be very sensitive to the external disturbance f_d . Both these two factors lead to a real system dynamics which is far from that of the nominal system. Thus it is necessary to use control system design methods which ensure the desired closed-loop stability and performance in the presence of uncertain parameters and disturbances.

Some realistic requirements of the closed-loop system dynamics, which have been considered in the design of the Disk Drive Servo using classical frequency response methods, are listed below

Table 2: Dynamic (resonance) parameters and tolerances

Parameter	Description	Value	Units	Tolerance
ω_1	resonance: VCM isolator	$2\pi 70$	rad/s	$\pm 5.0\%$
ω_2	resonance: head suspension	$2\pi 2200$	rad/s	$\pm 10.0\%$
ω_3	resonance: actuator arm carrier	$2\pi 4000$	rad/s	$\pm 5.0\%$
ω_4	resonance: coil structure	$2\pi 9000$	rad/s	$\pm 5.0\%$
b_1	first resonance coupling	-0.00575	-	$\pm 7.0\%$
b_2	first resonance coupling	-0.0000115	1/s	$\pm 7.0\%$
b_3	second resonance coupling	0.0230	-	$\pm 10.0\%$
b_4	second resonance coupling	0.0	1/s	$\pm 7.0\%$
b_5	third resonance coupling	0.8185	-	$\pm 5.0\%$
b_6	third resonance coupling	0.0	1/s	$\pm 10.0\%$
b_7	fourth resonance coupling	0.1642	-	$\pm 5.0\%$
b_8	fourth resonance coupling	0.0273	1/s	$\pm 10.0\%$
ξ_1	first resonance damping	0.05	-	$\pm 10.0\%$
ξ_2	second resonance damping	0.005	-	$\pm 40.0\%$
ξ_3	third resonance damping	0.05	-	$\pm 40.0\%$
ξ_4	fourth resonance damping	0.005	-	$\pm 50.0\%$

Peak closed-loop gain	$< 4 \text{ dB}$
Open-loop gain	$> 20 \text{ dB at } 100 \text{ Hz}$
Steady state error	$< 0.375 \text{ } \mu\text{m}$
Bandwidth	$> 800 \text{ Hz}$
Attenuation at 60 Hz	30 dB
Attenuation at 1.6 kHz	10 dB
Attenuation at 4 kHz	22 dB
Gain Margin	$> 10 \text{ dB}$
Phase margin	$> 45 \text{ deg}$

In addition, it is necessary to have smaller control action in order to avoid the power amplifier saturation.

3 Derivation of the uncertainty model

In order to implement robust control design methods we must have at our disposition a system model which involves the uncertain parameters. As it is seen from Table 1 and Table 2, the number of uncertain parameters is greater than 25, which complicates very much the analysis and design of the disk drive servo system. In this study we shall concentrate on those uncertainty parameters which influence most the closed loop system behaviour.

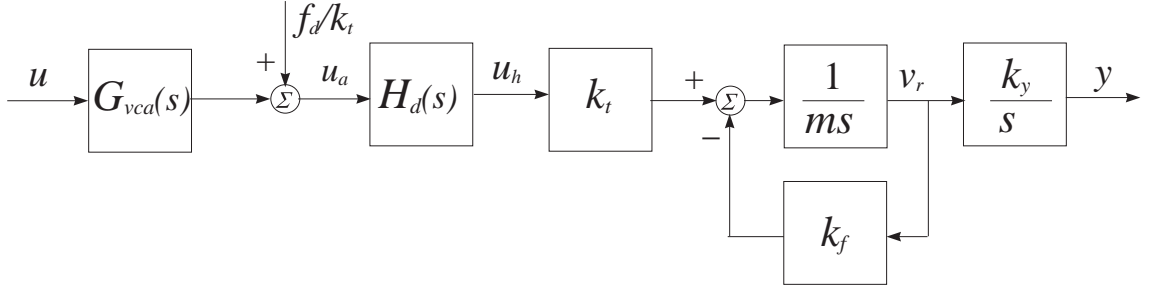


Figure 5: Transformed block diagram of the open-loop contour

For convenience, the open loop system blocks are rearranged as shown in Figure 5.

Consider first the derivation of the uncertainty model for the resonance modes. For each of the four modes we have the similar transfer function so we shall describe here only the first mode. Its state space model is (for the simplicity of notations we drop some subscripts)

$$\begin{aligned}\dot{x}_1 &= \omega x_2, \\ \dot{x}_2 &= \omega(-x_1 - 2\xi x_2 + u), \\ y_1 &= b_1 x_1 + b_2 x_2\end{aligned}$$

The block diagram of the state equations of a flexible mode is shown in Figure 6.

The variations in the frequency ω and the damping coefficient ξ are represented as

$$\omega = \bar{\omega}(1 + p_\omega \delta_\omega)$$

and

$$\xi = \bar{\xi}(1 + p_\xi \delta_\xi),$$

respectively, where $\bar{\omega}$ and $\bar{\xi}$ are the nominal values, p_ω and p_ξ are the maximum relative uncertainties and

$$-1 \leq \delta_\omega \leq 1,$$

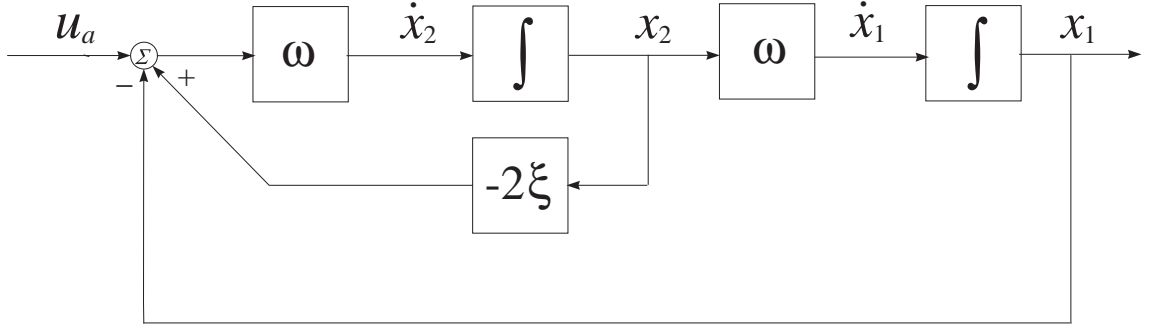


Figure 6: Block diagram of a flexible mode

$$-1 \leq \delta_\xi \leq 1$$

are the relative variations in these parameters.

The parameter ω may be represented as an upper Linear Fractional Transformation (LFT) in δ_ω

$$\omega = F_U(M_\omega, \delta_\omega)$$

with

$$M_\omega = \begin{bmatrix} 0 & \bar{\omega} \\ p_\omega & \bar{\omega} \end{bmatrix}$$

and the parameter ξ may be represented as an upper LFT in δ_ξ ,

$$\xi = F_U(M_\xi, \delta_\xi)$$

with

$$M_\xi = \begin{bmatrix} 0 & \bar{\xi} \\ p_\xi & \bar{\xi} \end{bmatrix}$$

(see [6], [3]).

The block diagram of a flexible mode with uncertain parameters is given in Figure 7. From this diagram we derive the following equations

$$\begin{bmatrix} y_\omega \\ \dot{x}_2 \end{bmatrix} = \begin{bmatrix} 0 & \bar{\omega} \\ p_\omega & \bar{\omega} \end{bmatrix} \begin{bmatrix} u_\omega \\ u - 2v_\xi - x_1 \end{bmatrix},$$

$$\begin{bmatrix} z_\omega \\ \dot{x}_1 \end{bmatrix} = \begin{bmatrix} 0 & \bar{\omega} \\ p_\omega & \bar{\omega} \end{bmatrix} \begin{bmatrix} v_\omega \\ x_2 \end{bmatrix},$$

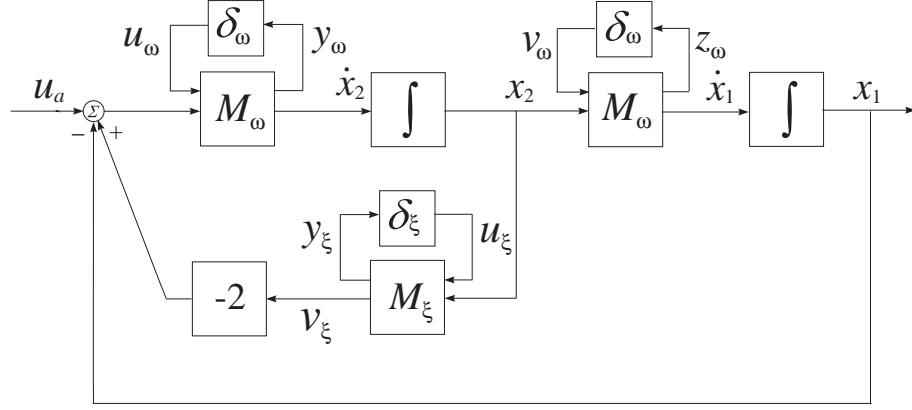


Figure 7: Flexible Mode with uncertain parameters

$$\begin{bmatrix} y_\xi \\ v_\xi \end{bmatrix} = \begin{bmatrix} 0 & \bar{\xi} \\ p_\omega & \bar{\xi} \end{bmatrix} \begin{bmatrix} u_\xi \\ x_2 \end{bmatrix},$$

and

$$y = \begin{bmatrix} b_1 & b_2 \end{bmatrix} \begin{bmatrix} x_1 \\ x_2 \end{bmatrix}.$$

From these equations we obtain the perturbed model of a flexible mode in the form of

$$\begin{bmatrix} \dot{x}_1 \\ \dot{x}_2 \\ \vdots \\ y_\omega \\ z_\omega \\ y_\xi \\ \vdots \\ y \end{bmatrix} = \begin{bmatrix} 0 & \bar{\omega} & | & 0 & p_\omega & 0 & | & 0 \\ -\bar{\omega} & -2\bar{\omega}\bar{\xi} & | & p_\omega & 0 & -2\bar{\omega}p_\xi & | & \bar{\omega} \\ \vdots & \vdots & | & \vdots & \vdots & \vdots & | & \vdots \\ -\bar{\omega} & -2\bar{\omega}\bar{\xi} & | & p_\omega & 0 & -2\bar{\omega}p_\xi & | & \bar{\omega} \\ 0 & \bar{\omega} & | & 0 & 0 & 0 & | & 0 \\ 0 & \bar{\xi} & | & 0 & 0 & 0 & | & 0 \\ \vdots & \vdots & | & \vdots & \vdots & \vdots & | & \vdots \\ b_1 & b_2 & | & 0 & 0 & 0 & | & 0 \end{bmatrix} \begin{bmatrix} x_1 \\ x_2 \\ \vdots \\ u_\omega \\ v_\omega \\ u_\xi \\ \vdots \\ u_a \end{bmatrix}.$$

A generalized block diagram of a flexible mode with four inputs and four outputs is shown in Figure 8.

Consider now the derivation of the uncertain model of the rigid body part of the system taking into account the viscous friction. The block diagram of this part of the system is shown in Figure 9. The state space equations in this case are

$$\begin{aligned} \dot{x}_1 &= k_y x_2, \\ \dot{x}_2 &= -\frac{k_f}{m} x_2 + \frac{k_t}{m} (y_1 + y_2 + y_3 + y_4). \end{aligned}$$

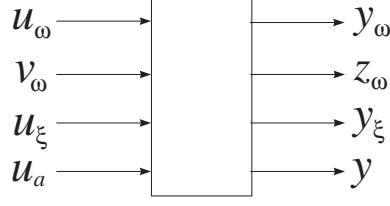


Figure 8: Generalized block diagram of a flexible mode

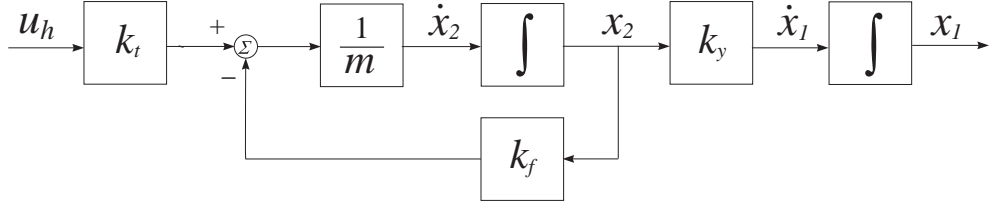


Figure 9: Block diagram of the rigid body model

The uncertain parameters of the rigid body model are taken as

$$\begin{aligned} k_t &= \bar{k}_t(1 + p_{k_t}\delta_{k_t}), \\ k_y &= \bar{k}_y(1 + p_{k_y}\delta_{k_y}), \\ k_f &= \bar{k}_f(1 + p_{k_f}\delta_{k_f}) \end{aligned}$$

with

$$-1 \leq \delta_{k_t} \leq 1,$$

$$-1 \leq \delta_{k_y} \leq 1,$$

$$-1 \leq \delta_{k_f} \leq 1.$$

These parameters are represented as LFT in the relative uncertainties δ_{k_t} , δ_{k_y} , δ_{k_f} :

$$\begin{aligned} k_t &= F_U(M_{k_t}, \delta_{k_t}), \\ k_y &= F_U(M_{k_y}, \delta_{k_y}), \\ k_f &= F_U(M_{k_f}, \delta_{k_f}), \end{aligned}$$

where

$$M_{k_t} = \begin{bmatrix} 0 & \bar{k}_t \\ p_{k_t} & \bar{k}_t \end{bmatrix}, \quad M_{k_y} = \begin{bmatrix} 0 & \bar{k}_y \\ p_{k_y} & \bar{k}_y \end{bmatrix}, \quad M_{k_f} = \begin{bmatrix} 0 & \bar{k}_f \\ p_{k_f} & \bar{k}_f \end{bmatrix}.$$

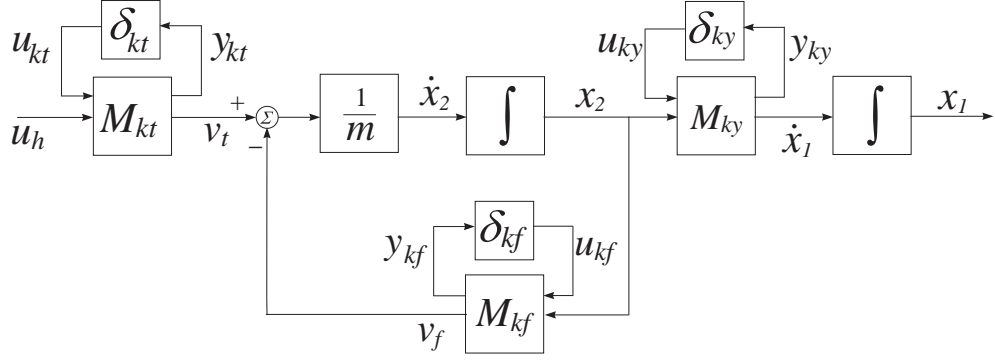


Figure 10: Rigid Body model with uncertain parameters

As a result we obtain the block diagram shown in Figure 10.

From this block diagram in a way similar to the case of a flexible mode we derive the following rigid body uncertainty model

$$\begin{bmatrix} \dot{x}_1 \\ \dot{x}_2 \\ \text{---} \\ y_{k_t} \\ y_{k_y} \\ y_{k_f} \\ \text{---} \\ y \end{bmatrix} = \begin{bmatrix} 0 & \bar{k}_y & | & 0 & p_{k_y} & 0 & | & 0 \\ 0 & -\frac{\bar{k}_f}{m} & | & \frac{p_{k_t}}{m} & 0 & -\frac{p_{k_f}}{m} & | & \frac{\bar{k}_t}{m} \\ \text{---} & \text{---} & \text{---} & \text{---} & \text{---} & \text{---} & \text{---} & \text{---} \\ 0 & 0 & | & 0 & 0 & 0 & | & \bar{k}_t \\ 0 & \bar{k}_y & | & 0 & 0 & 0 & | & 0 \\ 0 & \bar{k}_f & | & 0 & 0 & 0 & | & 0 \\ \text{---} & \text{---} & \text{---} & \text{---} & \text{---} & \text{---} & \text{---} & \text{---} \\ 1 & 0 & | & 0 & 0 & 0 & | & 0 \end{bmatrix} \begin{bmatrix} x_1 \\ x_2 \\ \text{---} \\ u_{k_t} \\ u_{k_y} \\ u_{k_f} \\ \text{---} \\ u_h \end{bmatrix}.$$

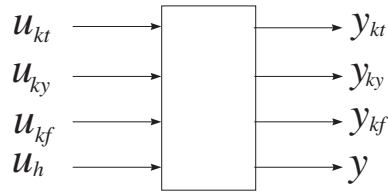


Figure 11: Generalized block diagram of the Rigid Body model with uncertain parameters

The generalized block diagram of the rigid body model with four inputs and four outputs is shown in Figure 11.

Now we may connect the uncertain models of the four resonance modes with the uncertain

model of the rigid body, as shown in Figure 12.

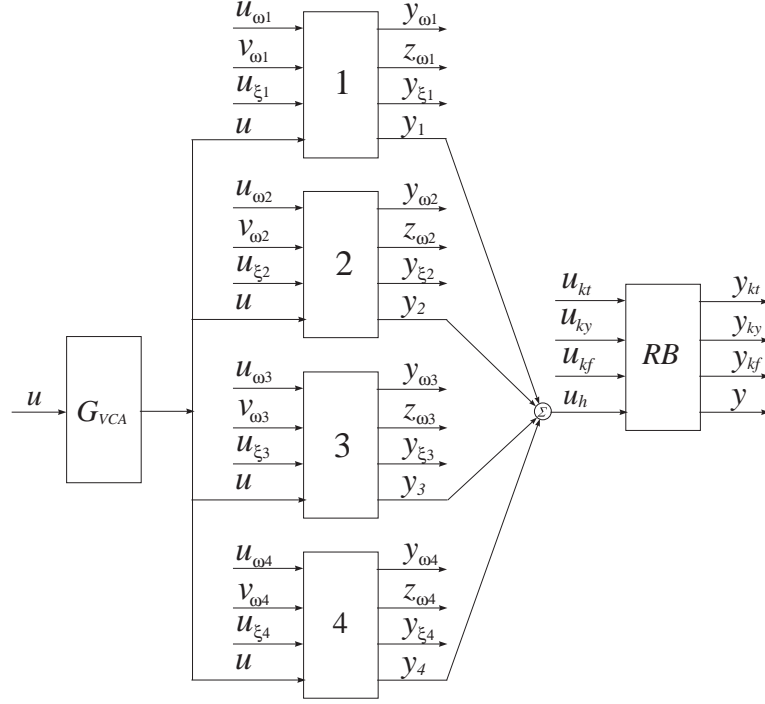


Figure 12: Plant model with uncertainties

Overall, we have eleven uncertain parameters but four of them (ω_1 , ω_2 , ω_3 and ω_4) are repeated twice.

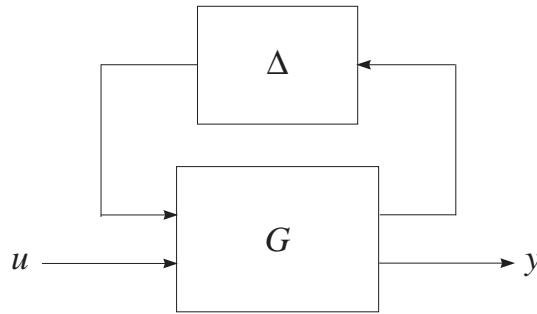


Figure 13: Plant model in the form of an upper LFT

By 'puling out' the uncertain parameters from the nominal part of the model we obtain a perturbed plant model in the form of an upper LFT as shown in Figure 13 with a 15×15 matrix

Δ ,

$$\Delta = \text{diag}(\delta_{\omega_1}, \delta_{\omega_1}, \delta_{\xi_1}, \delta_{\omega_2}, \delta_{\omega_2}, \delta_{\xi_2}, \delta_{\omega_3}, \delta_{\omega_3}, \delta_{\xi_3}, \delta_{\omega_4}, \delta_{\omega_4}, \delta_{\xi_4}, \delta_{k_t}, \delta_{k_y}, \delta_{k_f}),$$

which contains the uncertain parameters.

The system model is of order twelve.

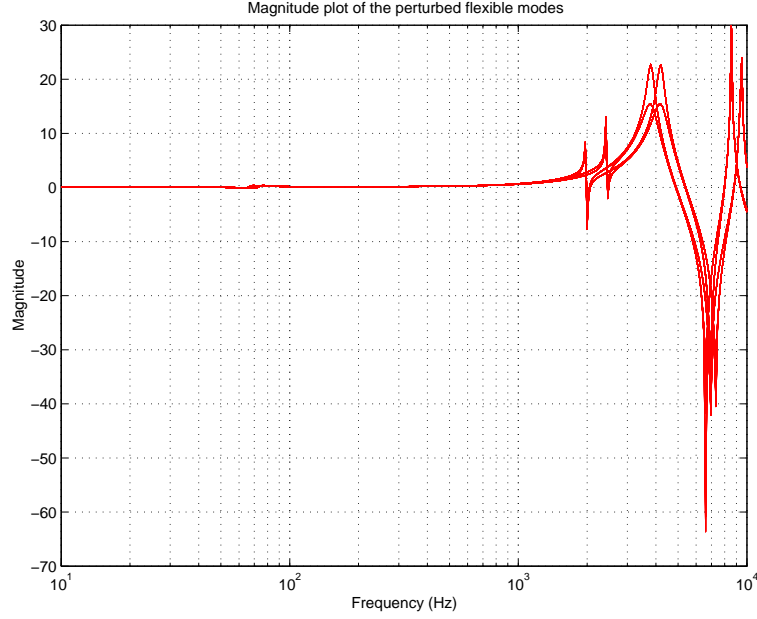


Figure 14: Magnitude plot of the perturbed flexible modes

In Figures 14 and 15 we show the Bode plot of the parallel connection $H_d(s)$ of the flexible modes with uncertain parameters varying between the lower and upper bounds.

4 Closed-loop system performance requirements

The block diagram of the closed-loop system, which includes the feedback structure and the controller as well as the elements reflecting the model uncertainty and the performance objectives, is shown in Figure 16.

The system has a reference input (r), an input disturbance (d) and two output costs (e_y and e_u). The system M is an ideal model to match the closed loop system to. The rectangle, shown with dash line, represents the plant transfer function matrix G . Inside the rectangle is the nominal model G_{nom} of the disk drive control system and the block Δ , which parameterizes the model uncertainties. The matrix Δ is unknown, but it has a diagonal structure and norm bound

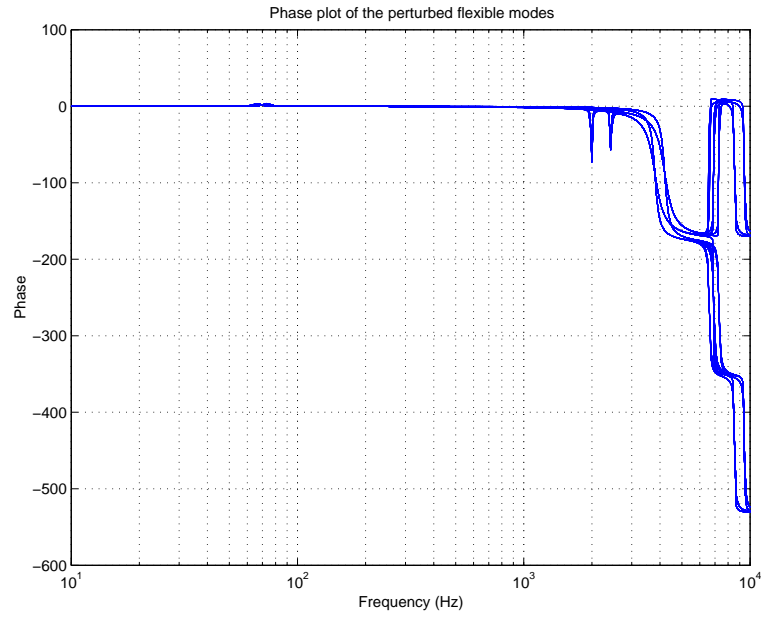


Figure 15: Phase plot of the perturbed flexible modes

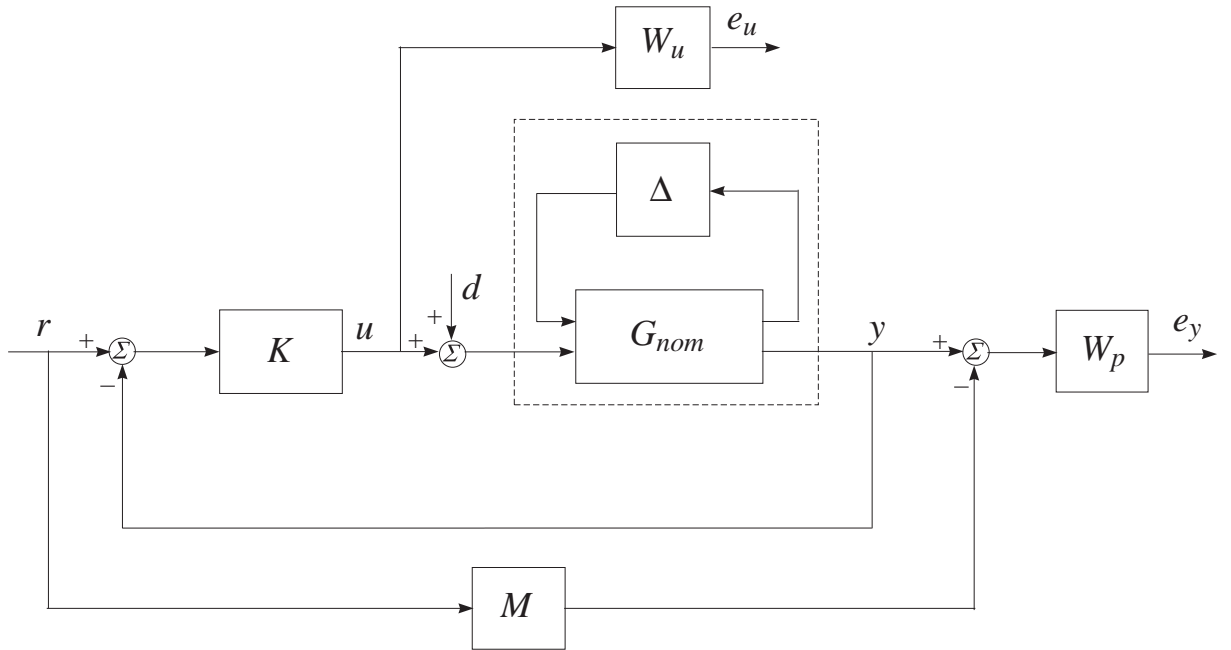


Figure 16: Closed-loop system with performance specifications

$\|\Delta\|_\infty < 1$. The performance objective requires the transfer matrices from r and d to e_y and e_u to be small in the sense of $\|\cdot\|_\infty$, for all possible uncertain matrices Δ . The transfer matrices W_p and W_u are used to reflect the relative significance of the different frequency ranges for which the performance is required. Hence, the performance objective can be recast, with possible slight conservativeness, as that the $\|\cdot\|_\infty$ of the transfer function matrix from r and d to e_y and e_u is less than 1.

It is a routine manipulation to show that

$$\begin{bmatrix} e_y \\ e_u \end{bmatrix} = \begin{bmatrix} W_p(S_o G K - M) & W_p S_o G \\ W_u S_i K & -W_u K S_o G \end{bmatrix} \begin{bmatrix} r \\ d \end{bmatrix}$$

where $S_i = (I + K G)^{-1}$, $S_o = (I + G K)^{-1}$ are the input and output sensitivities, respectively. Note that $S_o G$ is the transfer function between d and y .

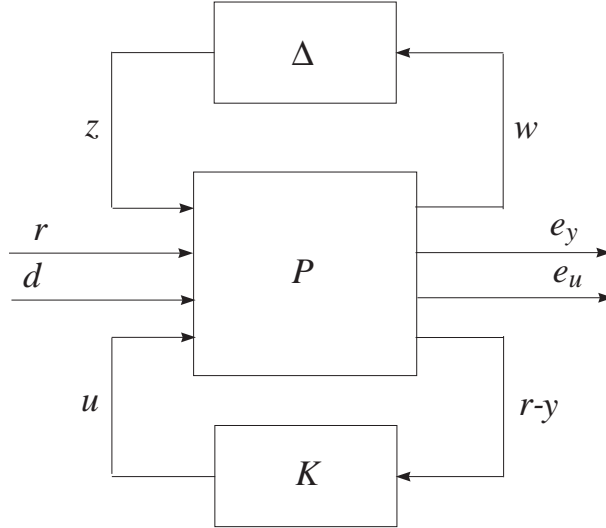


Figure 17: Total interconnection structure of the closed-loop system

Based on Figure 16, the total interconnection block diagram of the closed-loop system is shown in Figure 17. The transfer function matrix P is determined by the matrices G_{nom} , W_p and W_u . w and z denote the inputs to and outputs from the uncertainty block Δ , respectively.

The controller synthesis problem of the Disk Drive Servo System is to find a linear, output feedback, controller $K(s)$ which has to ensure the following properties of the closed-loop system.

Nominal performance: The closed-loop system achieves nominal performance if the performance objective is satisfied for the nominal plant model.

The performance objective is to satisfy the inequality

$$\left\| \begin{bmatrix} W_p(S_o G_{nom} K - M) & W_p S_o G_{nom} \\ W_u S_i K & -W_u K S_o G_{nom} \end{bmatrix} \right\|_{\infty} < 1 \quad (4.1)$$

This objective is similar to the usual mixed S/KS sensitivity optimization and it enables robustness and performance criteria to be met incorporating performance specifications in the matching model M . The four functions to be minimized are described in Table 3.

Table 3: \mathcal{H}_{∞} functions to be minimized

Function	Description
$W_p(S_o G K - M)$	Weighted difference between the ideal and actual closed systems
$W_p S_o G$	Weighted disturbance sensitivity
$W_u S_i K$	Weighted control effort due to reference input
$W_u K S_o G$	Weighted control effort due to the disturbance

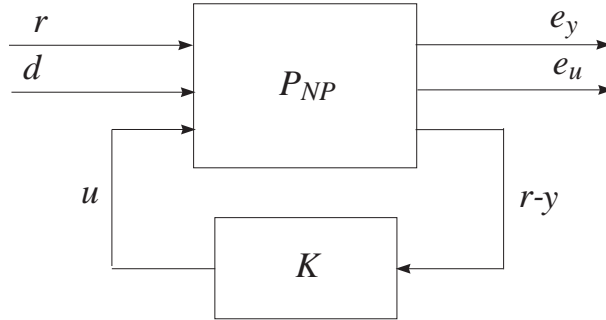


Figure 18: Interconnection structure, corresponding to nominal performance

The interconnection structure, corresponding to the nominal performance analysis, is shown in Figure 18. The transfer function matrix P_{NP} is determined from the matrix P , shown in Figure 17, neglecting the inputs to and the outputs from the uncertainty block Δ .

Robust stability: The closed-loop system achieves robust stability if the closed-loop system is internally stable for each possible plant dynamics $G = F_U(G_{nom}, \Delta)$.

The interconnection structure, corresponding to the robust stability analysis, is shown in Figure 19. The transfer function matrix P_{RS} is determined from the matrix P , shown in Figure 17, neglecting the inputs r, d and the outputs e_y, e_u .

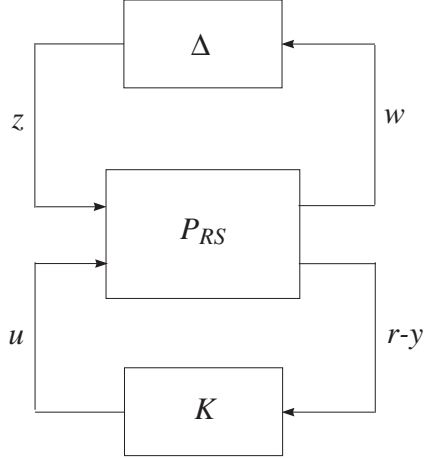


Figure 19: Interconnection structure, corresponding to robust stability

Robust performance: The closed-loop system must remain internally stable for each $G = F_U(G_{nom}, \Delta)$ and in addition the performance objective

$$\left\| \begin{bmatrix} W_p(S_o G K - M) & W_p S_o G \\ W_u S_i K & -W_u K S_o G \end{bmatrix} \right\|_{\infty} < 1 \quad (4.2)$$

should be satisfied for each $G = F_U(G_{nom}, \Delta)$. This means that the structured singular value, corresponding to the transfer function matrix from (Figure 17) $\begin{bmatrix} z \\ r \\ d \end{bmatrix}$ to $\begin{bmatrix} w \\ e_y \\ e_u \end{bmatrix}$ should be less

than 1, with regard to $\begin{bmatrix} \Delta & 0 \\ 0 & \Delta_F \end{bmatrix}$ where Δ_F is a fictitious 2×2 complex uncertainty block.

In addition to those requirements it is desirable that the controller designed would have acceptable complexity, i.e. it is of reasonably low order.

According to the above considerations, the aim of the design is to determine a controller K , such that for all stable perturbations Δ with $\|\Delta\|_{\infty} < 1$, the perturbed closed-loop system remains stable and the performance objective is satisfied for all such perturbations.

In the given case the ideal model is taken as

$$M = \frac{1}{5 \times 10^{-8} s^2 + 2.2 \times 10^{-4} s + 1}$$

and the weighting performance functions are chosen as

$$W_p(s) = \frac{s^2 + 1.10 \times 10^5 s + 3.6 \times 10^8}{s^2 + 1.00 \times 10^5 s + 3.6 \times 10^5}, \quad W_u(s) = 0.036.$$

The model transfer function is chosen so as the time response to the reference signal to have an overshoot less than 20% and a settling time less than 1.5 *ms*. The weighting functions are chosen so as to ensure an acceptable trade-off between the nominal performance and the robust performance of the closed-loop system.

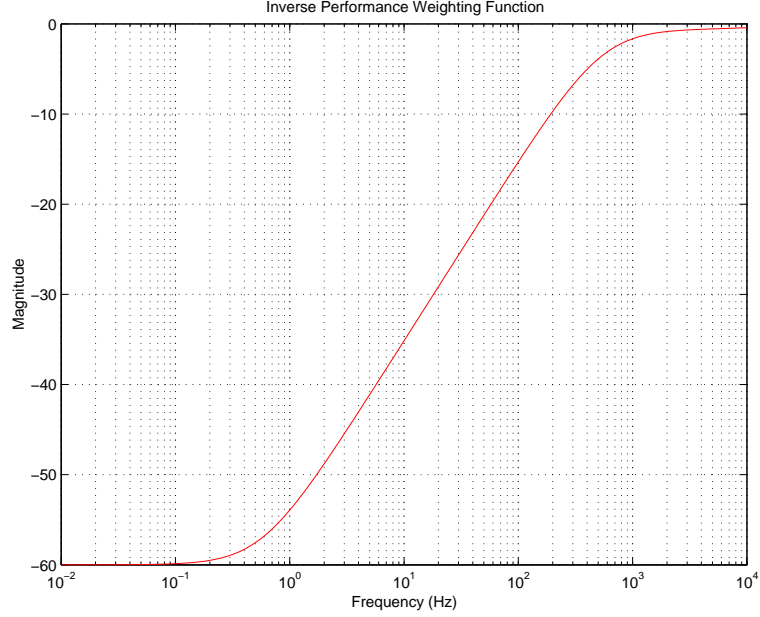


Figure 20: Frequency response of the inverse weighting function

In Figure 20 we show the frequency response of the inverse performance weighting function W_p^{-1} . It is seen that in the low frequency range we want the difference between the system and model outputs and the effect of the disturbance on the system output both to be very small. This will ensure good tracking of the reference input and small error due to low-frequency disturbances.

The internal structure of the seventeen input seventeen output system of order sixteen, which is saved as the variable `sys_ic`, is shown in Figure 21. The inputs and outputs of the uncertainties are saved as the variables `pertin` and `pertout`, the reference and the disturbance - as the variables `ref` and `dist` and the control - as the variable `control`.

Both variables `pertin` and `pertout` have fifteen elements and `ref`, `dist`, `y`, `y_c`, `e_y` and `e_u` are scalar variables.

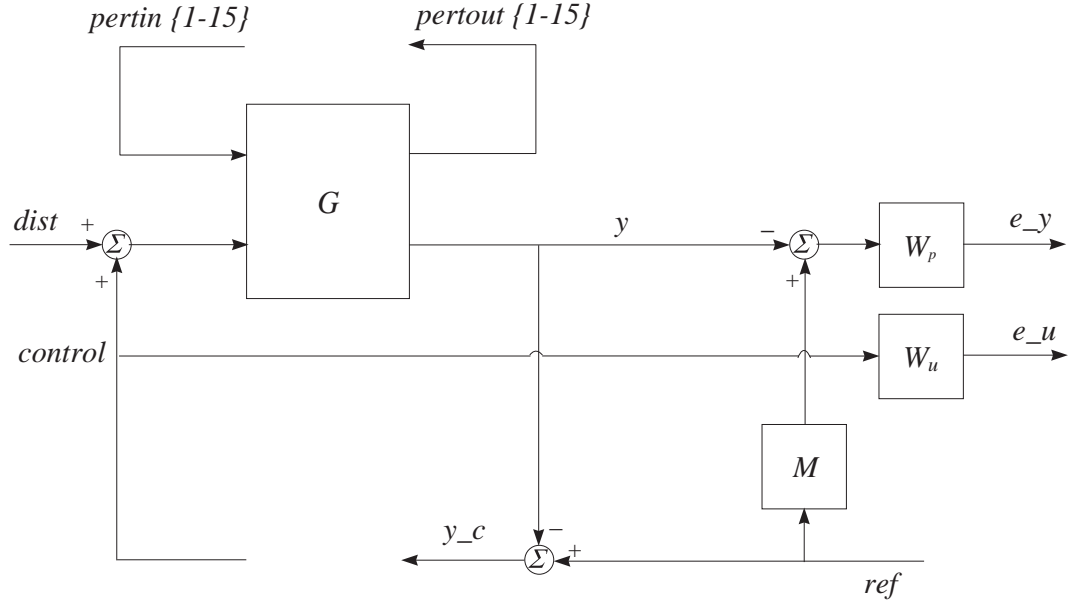


Figure 21: Open-loop system with performance specifications

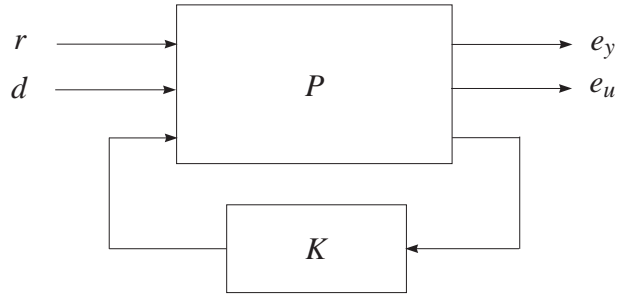


Figure 22: Closed-loop system with H_∞ controller

5 \mathcal{H}_∞ design

The aim of the design in this case is to find an \mathcal{H}_∞ (sub)optimal output controller for the interconnection shown in Figure 22 in which we neglect the inputs and outputs of the uncertainty. The variable `hin_ic` which corresponds to the transfer function P of the open-loop system may be obtained by the line

```
hin_ic = sel(sys_ic,[16:18],[16:18])
```

The \mathcal{H}_∞ optimal control minimizes the $\|\cdot\|_\infty$ -norm of $F_L(P, K)$ in respect to the transfer function K of the controller. In the given case $F_L(P, K)$ is the nominal closed-loop transfer function matrix

from the reference and disturbance signals (the variables **ref** and **dist**) to the outputs **e_y** and **e_u** of the weighting functions. The design is done by the SLICOT mex-file **conhin**, which computes a (sub)optimal H_∞ control law for the given open-loop system. The value of γ is chosen 1.6045 which is slightly above the minimum possible value. The controller obtained is of 16-th order.

The test for robust stability is done on the upper 15×15 block of the closed-loop transfer function matrix. To achieve robust stability it is necessary for each value of the frequency the μ bound to be less than 1.

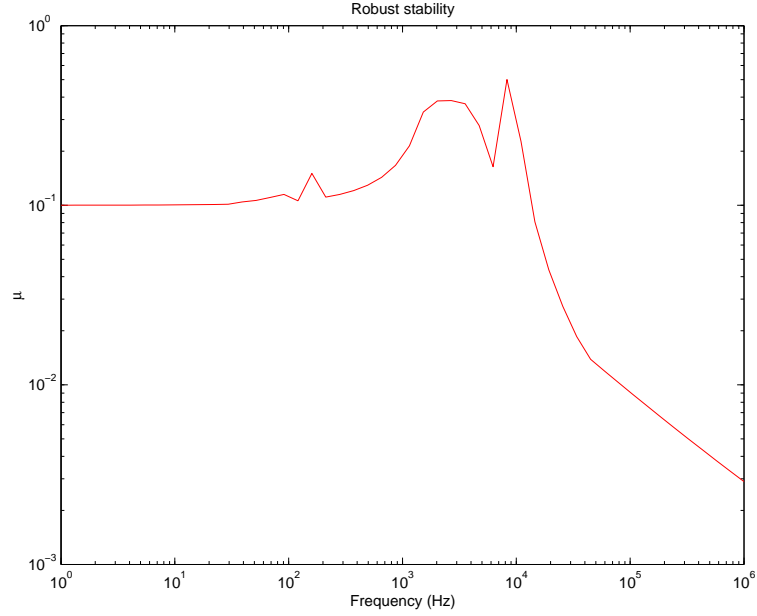


Figure 23: Robust stability of the closed-loop system for K_{hin}

The frequency response plot of the structured singular value for the case of robust stability is computed by using of the SLICOT mex-file **mucomp** and is shown in Figure 23. The maximum value of μ is 0.5014 which means that the stability of the closed-loop system is preserved under perturbations which satisfy $\|\Delta\|_\infty < \frac{1}{0.5014}$.

The test for nominal performance is done on the bottom 2×2 block of the closed-loop transfer function matrix. From the frequency response of the nominal performance shown in Figure 24 it follows that the nominal performance is almost achieved. This follows from the fact that the value of γ is close to 1.

The robust performance of the closed-loop system with \mathcal{H}_∞ controller is studied also by the aid of the μ -analysis. The closed-loop transfer function matrix has 17 inputs and 17 outputs. The

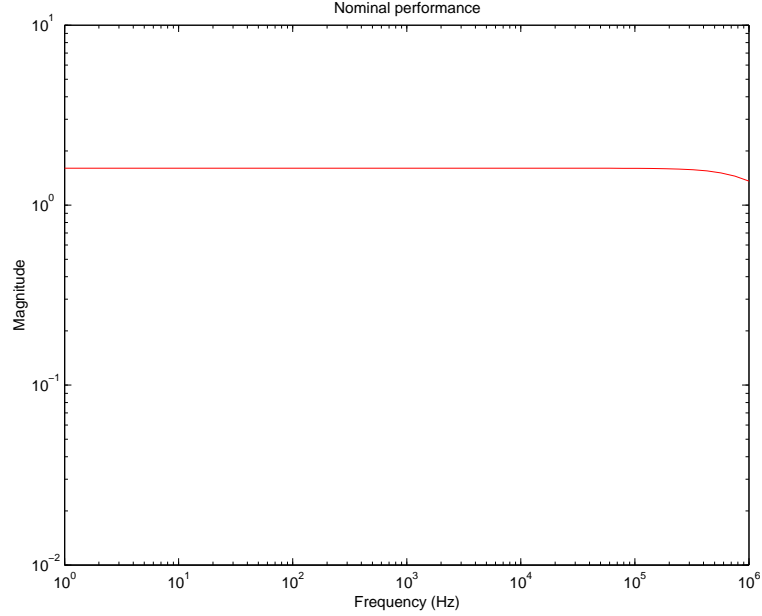


Figure 24: Nominal performance of the closed-loop system for K_{hin}

first 15 inputs/outputs correspond to the 15 channels which the perturbation Δ connects, while the last 2 inputs and outputs correspond to the weighted sensitivity of the closed-loop system. Hence, for a μ -analysis of the robust performance the block-structure of the uncertainty should consist of 15×15 diagonal real uncertainty block and 2×2 complex uncertainty block.

$$\Delta_P := \left\{ \begin{bmatrix} \Delta & 0 \\ 0 & \Delta_F \end{bmatrix} : \Delta \in \mathcal{C}^{15 \times 15}, \Delta_F \in \mathcal{C}^{2 \times 2} \right\}$$

The robust performance (in respect to the uncertainty and performance weighting functions) is achieved if and only if for each frequency $\mu_{\Delta_P}(\cdot)$, computed for the closed-loop frequency response is less than 1.

The frequency response plot of μ in the case of robust performance analysis is given in Figure 25. The maximum value of μ is 1.8217 and this shows that the performance specifications can not be met entirely for all possible parameter variations. However, from practical point of view the worst combination of parameter changes rarely occurs and with this value of μ we may safely accept that the system performance is robust.

In Figure 26 we show the transient response of the closed-loop system for a reference equivalent of 1 track ($12.5 \mu m$). We see that the overshoot 59% and the settling time (with respect to 5% zone around the steady state) is 2.98 ms so that the transient response is not entirely satisfactory.

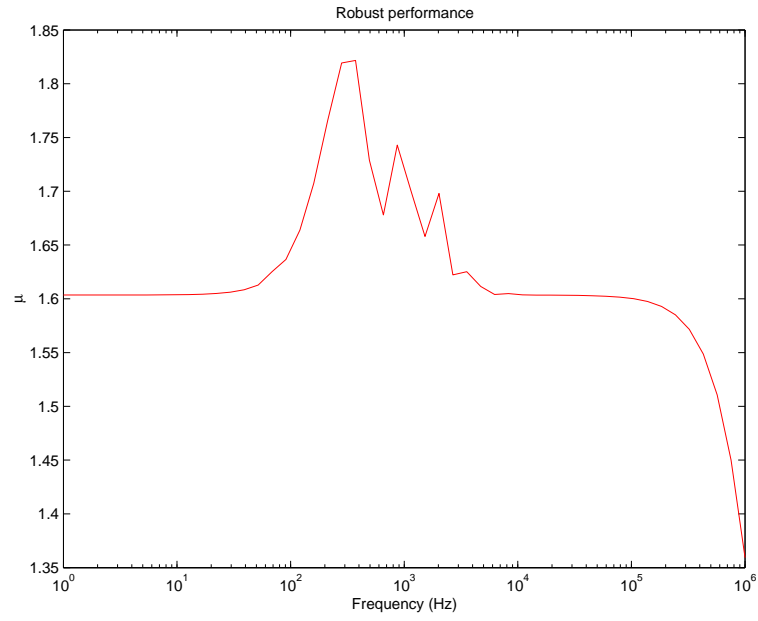


Figure 25: Robust performance of the closed-loop system for K_{hin}

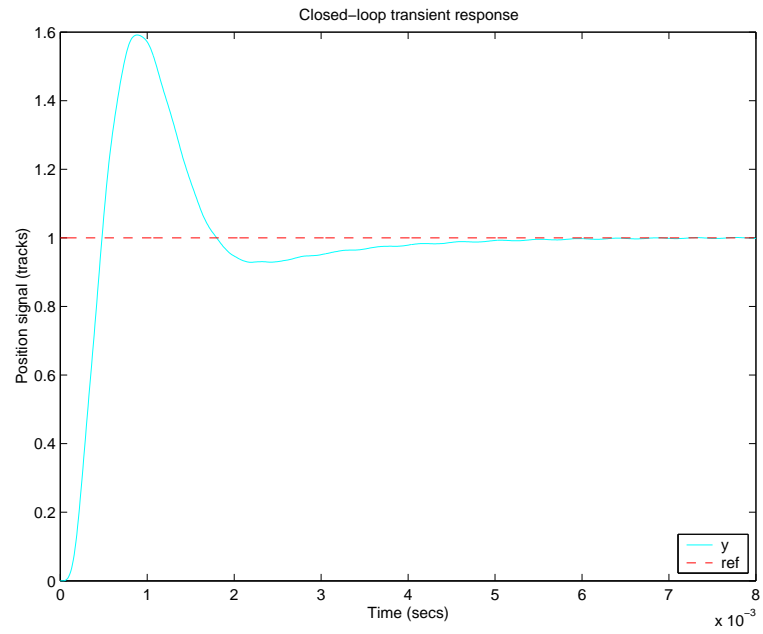


Figure 26: Transient response of the closed-loop system for K_{hin}

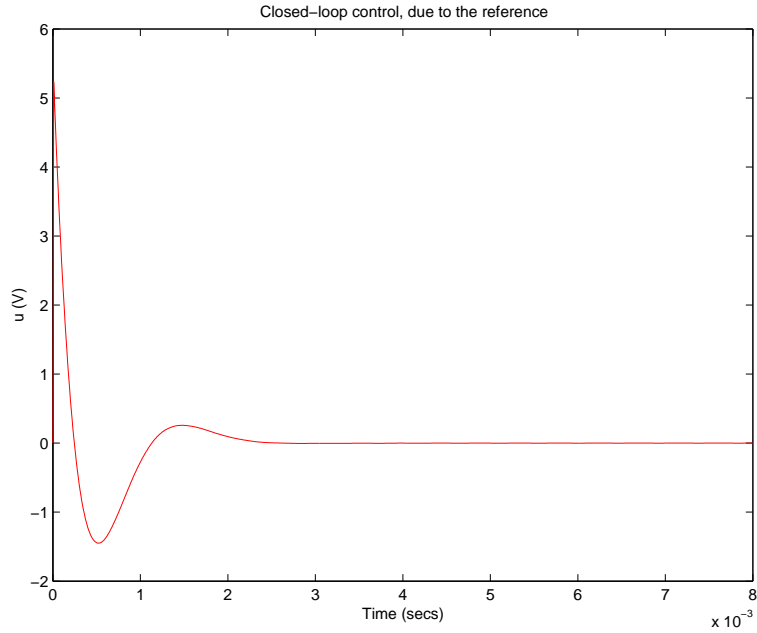


Figure 27: Control action for K_{hin}

The maximum of the control action (Figure 27) is 5.23 V and it is slightly larger than the value for which the amplifier saturates. This means that the actual transient response of the nonlinear system might be worse than this of the linearized system.

In Figure 28 we show the system response to a step disturbance (a force of 1N applied to the Disk Head Assembly). The transient error is less than 7% of the track width and the steady state error is practically equal to zero.

6 Loop Shaping Design

The design of a robust control for the Disk Drive System can be successfully done using also the Loop Shaping Design (LSHD) technique. This technique along with the algorithm implemented in SLICOT is described in [5], [9]. Note that in the case of LSHD we didn't use the performance specifications implemented in the case of \mathcal{H}_∞ design. Instead of these specifications we use a pre-filter W_1 and a post-filter W_2 in order to shape appropriately the open-loop transfer function W_1GW_2 .

In the present case we choose a pre-filter with transfer function

$$W_1 = 4 \frac{5s + 1}{s}$$

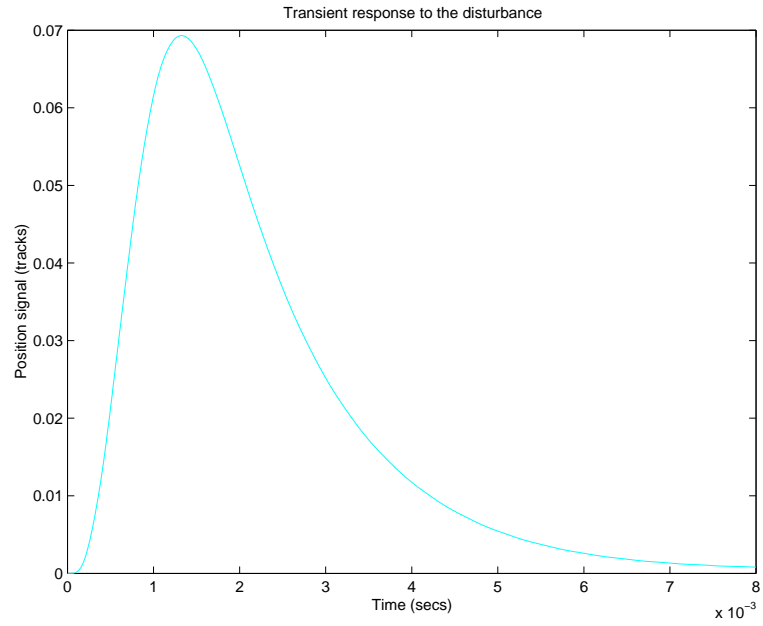


Figure 28: Disturbance response of the closed-loop system for K_{hin}

and we take the post-filter as $W_2 = 1$.

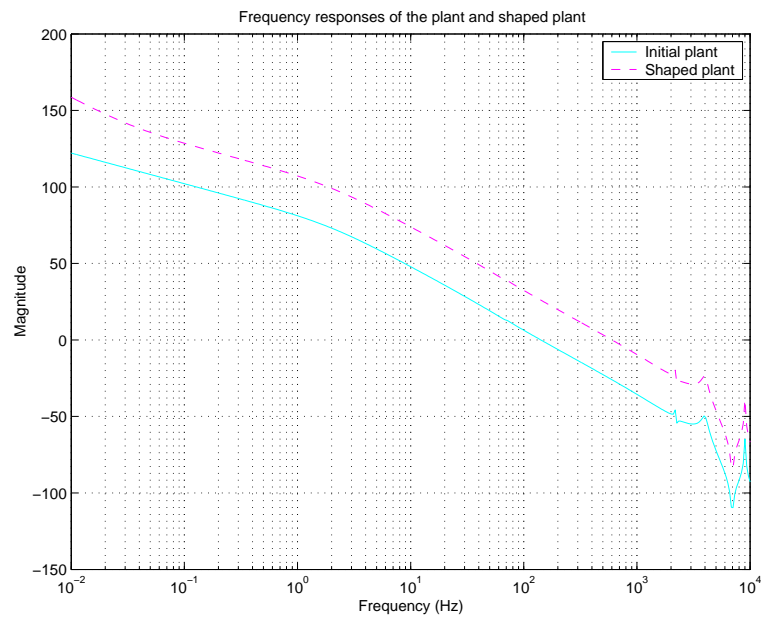


Figure 29: Magnitude plots of the original and shaped systems

The magnitude plots of the original and shaped systems are shown in Figure 29. The design of the LSHD controller is done using the SLICOT mex-file `clsdp` with $factor = 1.1$ which leads to a solution slightly different from the optimal one. The controller obtained is of order 14 (the order of the plant plus the order of the pre-filter).

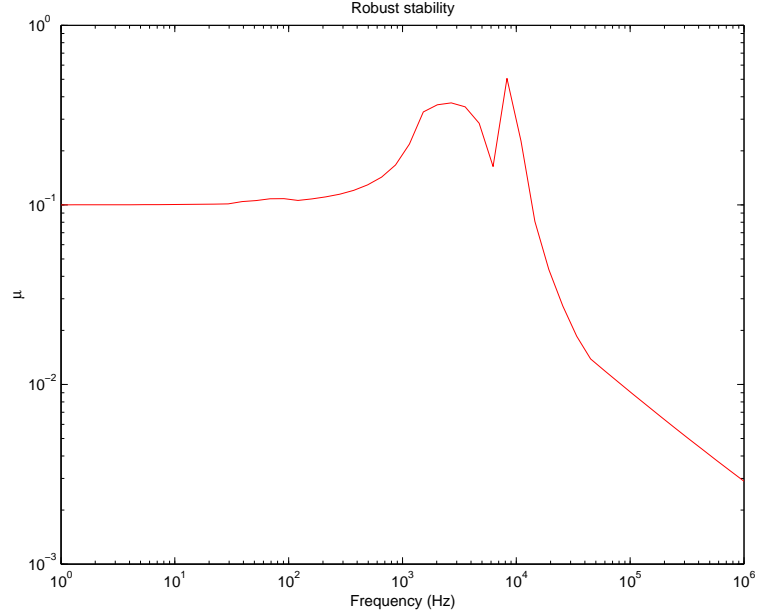


Figure 30: Robust stability of the closed-loop system with K_{lsh}

In Figure 30 we present the structured singular value plot for the robust stability analysis of the closed-loop systems with LSHD controller. We see from the Figure that the closed-loop system is robustly stable. The maximum value of μ for the Loop Shaping Design controller is 0.50618 which is close to the corresponding value for the \mathcal{H}_∞ controller.

The nominal performance and robust performance for the LSHD controller are shown in Figures 31 and 32, respectively. The bad performance in the low frequency range means that the error due to a low frequency disturbance will be large.

The transient response of the closed-loop system with LSHD controller is shown in Figure 33. The overshoot is 53% and is smaller than in the case of \mathcal{H}_∞ controller. The response is faster than in the case of \mathcal{H}_∞ controller the settling time being about 1.5 ms. In this way the transient response of the closed-loop system is very good.

The control action (Figure 34) of the LSHD controller has a maximum value which is equal to 4.7 V. This ensures a dynamics of the real system close to the dynamics of the linearized system.

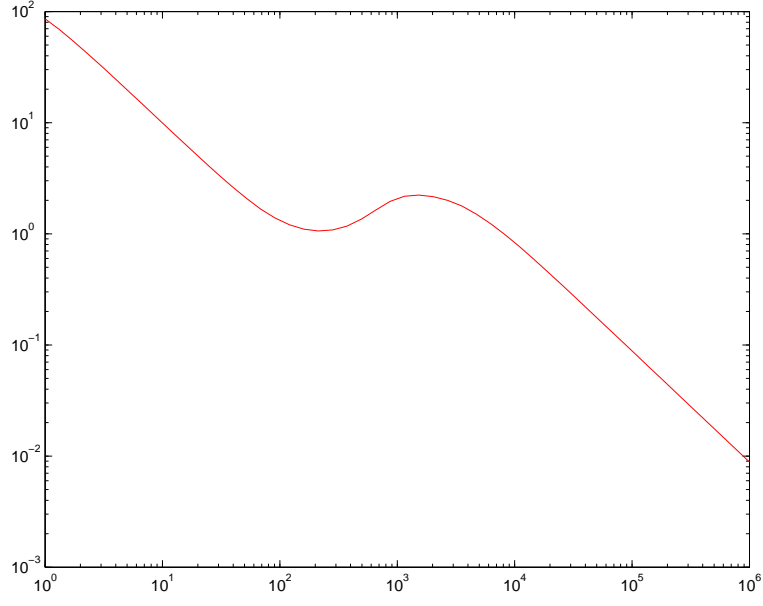


Figure 31: Nominal performance of the closed-loop system for K_{lsh}

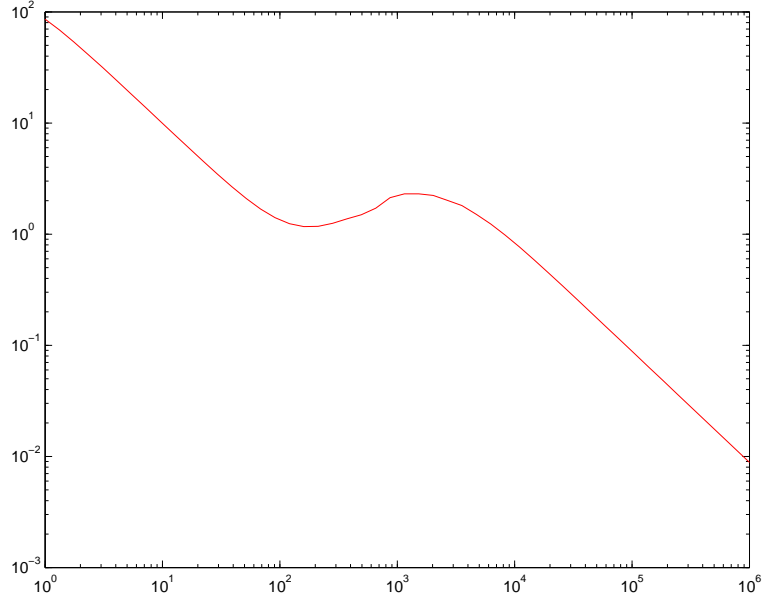


Figure 32: Robust performance of the closed-loop system for K_{lsh}

The disturbance response (Figure 35) of the closed-loop system with LSHD controller, obtained for $d = 1\ N$, has a relatively large steady-state value which is more than 7% of the track width.

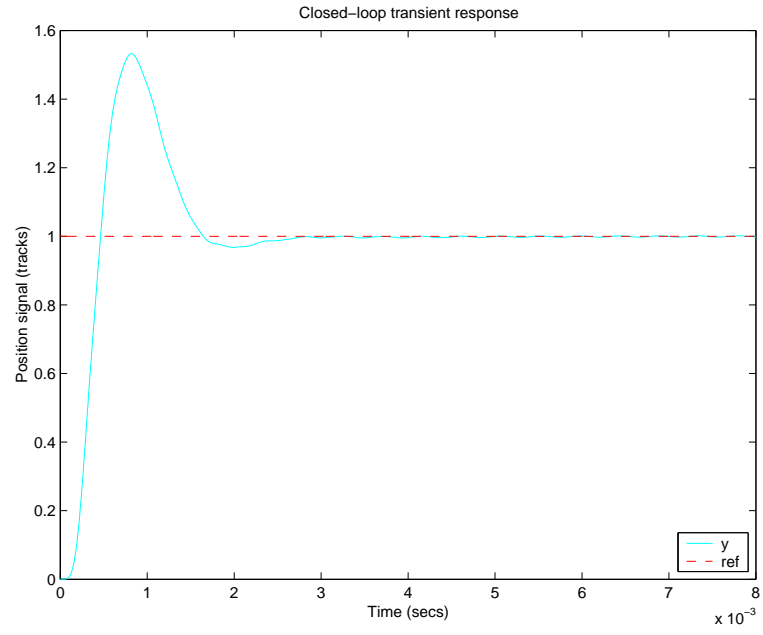


Figure 33: Transient response of the closed-loop system for K_{lsh}

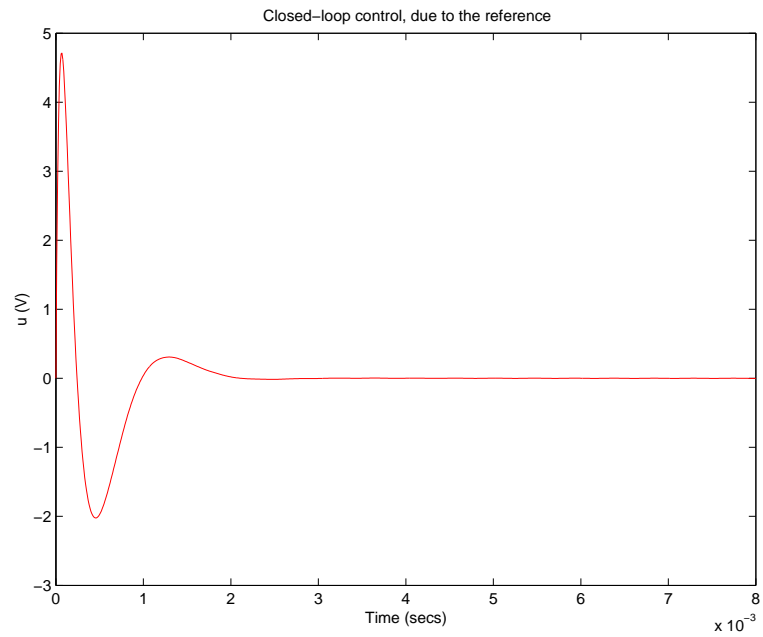


Figure 34: Control action for K_{lsh}

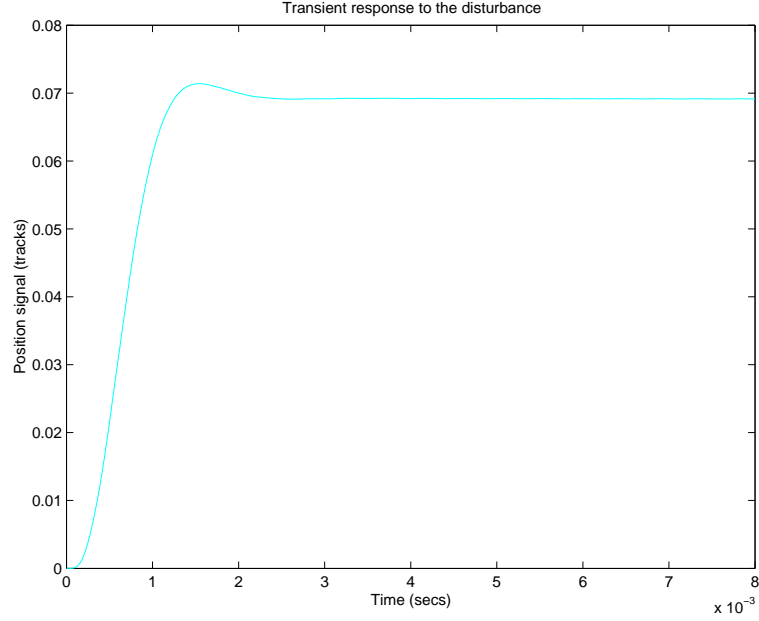


Figure 35: Disturbance response of the closed-loop system for K_{lsh}

7 μ -design

The design of the Disk Drive Servo Control System may be done also by the μ -synthesis which usually leads to better performance and robustness in comparison to \mathcal{H}_∞ optimisation. In the μ -synthesis it is necessary to use inputs and outputs of the uncertainty blocks which gives more freedom in the design. In the given case we shall use only the inputs and outputs of the uncertainty in the rigid body model, since the adding of the rest inputs and outputs makes the D_K iterations nonconvergent. It is necessary to mention that the negligence of some inputs and outputs does not mean that the dynamics of the corresponding blocks in the plant model is also neglected.

The block diagram of the closed loop system used in the μ synthesis is shown in Figure 36. Denote by $P(s)$ the transfer matrix of the five input, five output open loop system `nominal_dk` and let the block structure of the uncertainty Δ_P is defined as

$$\Delta_P := \left\{ \begin{bmatrix} \Delta_r & 0 \\ 0 & \Delta_F \end{bmatrix} : \Delta_r \in \mathcal{R}^{3 \times 3}, \Delta_F \in \mathcal{C}^{2 \times 2} \right\}$$

The first block of this matrix corresponds to the block Δ_r containing the uncertainties in the rigid body model. The second block Δ_F is a fictitious uncertainty block which is used to implement the performance requirements in the framework of the μ approach. In order to satisfy the performance requirements it is necessary to find a stabilizing controller $K(s)$, such that for each frequency

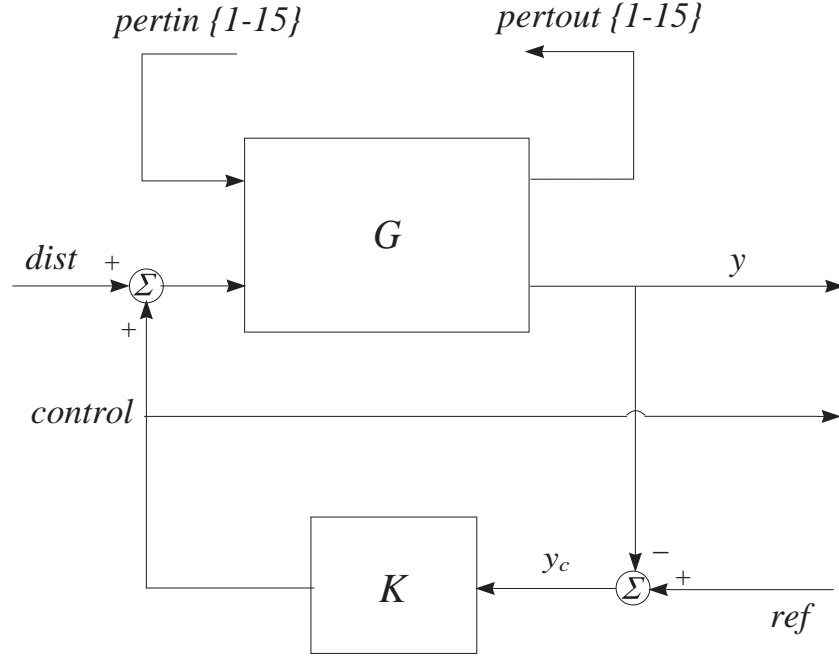


Figure 36: Closed loop system with μ controller

$\omega \in [0, \infty]$ the structured singular value satisfies the condition

$$\mu_{\Delta_P}[F_L(P, K)(j\omega)] < 1.$$

The fulfillment of this condition guaranties robust stability of the closed-loop system, i.e.

$$\left\| \begin{bmatrix} W_p(S_o G K - M) & W_p S_o G \\ W_u S_i K & -W_u K S_o G \end{bmatrix} \right\|_{\infty} < 1. \quad (7.3)$$

The μ -synthesis is done by using the SLICOT mex-file **mucomp** implementing some of the commands from **μ -toolbox**. The order of the controllers and the maximum value of μ for each iteration are given in Table 4.

We see from the Table that after the fifth iteration the maximum value of μ is equal to 1.767, which means that the corresponding closed loop system is near to achieve robust performance. *It is necessary to note that the robust performance achieved is only with respect to the uncertainties in the rigid body model, since only these uncertainties are taken into account in the design. Hence it is necessary to make additional robust stability analysis taking also into account the rest uncertainties.*

The final controller is of 38-th order.

The frequency response of the structured singular value for the case of robust stability is shown in Figure 37. The maximum value of μ is 0.50016 which means that the stability of the

Table 4: Results from D-K-iterations

Iteration	Controller order	Maximum value of μ
1	16	969.372
2	20	14.532
3	32	3.602
4	32	2.105
5	38	1.767

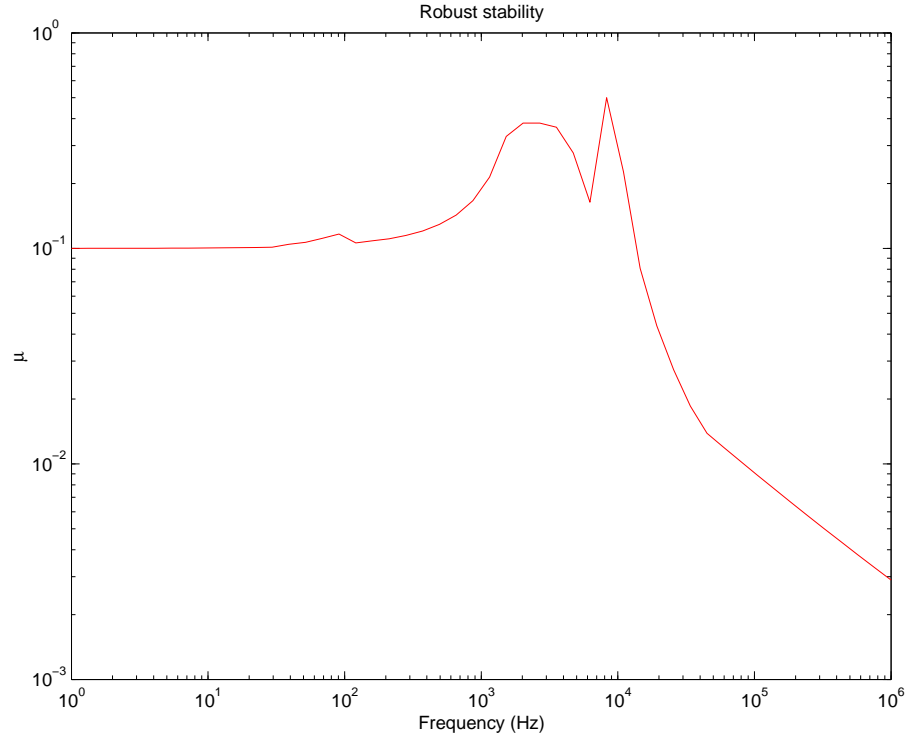


Figure 37: Robust stability of the closed loop system for K_μ

closed-loop system is preserved under perturbations which satisfy $\|\Delta\|_\infty < \frac{1}{0.50016}$. In this way the robust stability of the closed loop system is achieved independently on the fact that some of the uncertainties were neglected during the μ -synthesis.

In Figure 38 we show the individual contributions to μ due to the different uncertainties. It is seen that the contribution of each flexible mode has a maximum for the corresponding resonance

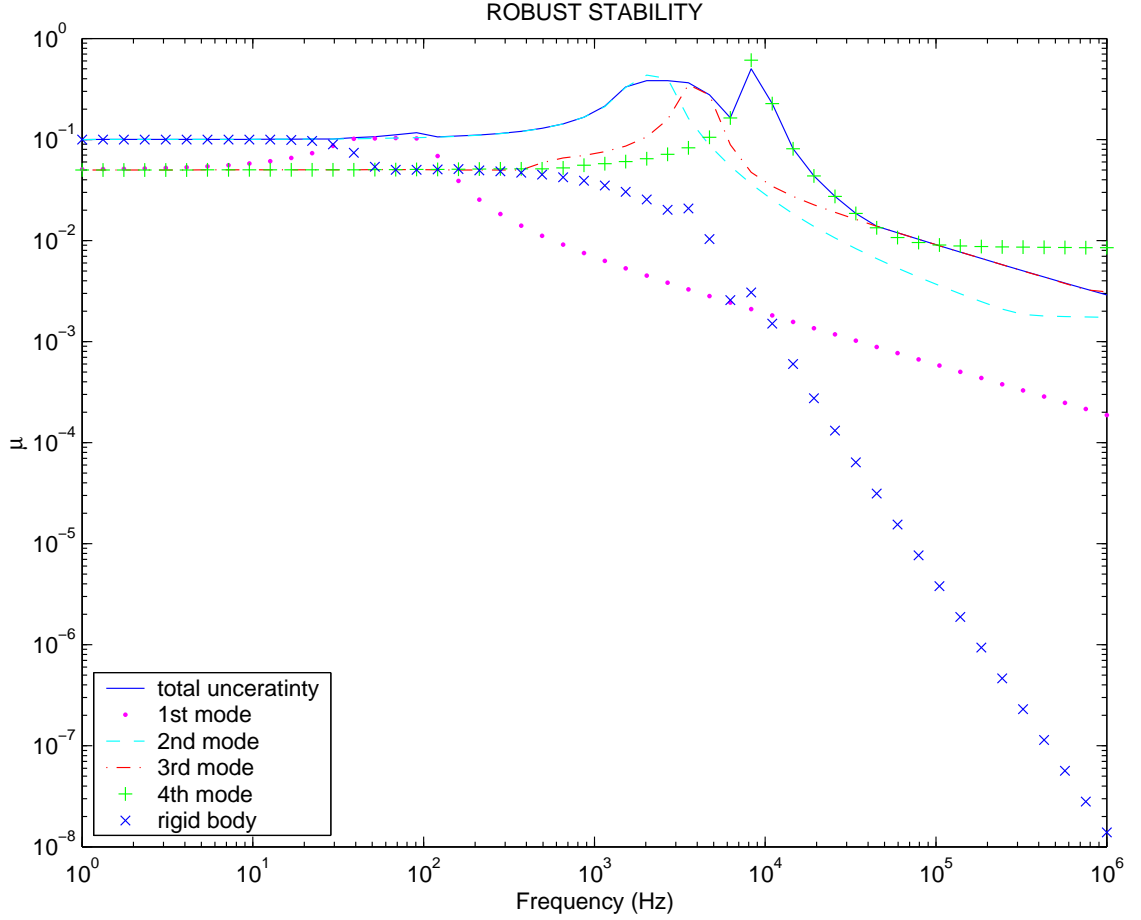


Figure 38: Contribution of the uncertainties to the robust stability

frequency.

The frequency responses of the nominal and robust performance are shown in Figures 39 and 40, respectively. The closed loop system is near to achieve robust performance since the maximum value of μ in this case is 1.8306.

The Bode plot of the closed-loop system is shown in Figures 41 and 42. For low frequencies the value of the magnitude plot is very close to 1 which implies good reference tracking. The peak of the magnitude plot is less than 5 dB and the bandwidth (at -3 dB level) is 1000 Hz. The gain margin and phase margin are 11 dB and 35 deg, respectively.

From the magnitude plot of the sensitivity function frequency response, given in Figure 43, we see that the sensitivity plot is laying slightly above the magnitude plot of the inverse weighting function W_p^{-1} , i.e. the requirements to the sensitivity are almost satisfied. The disturbance

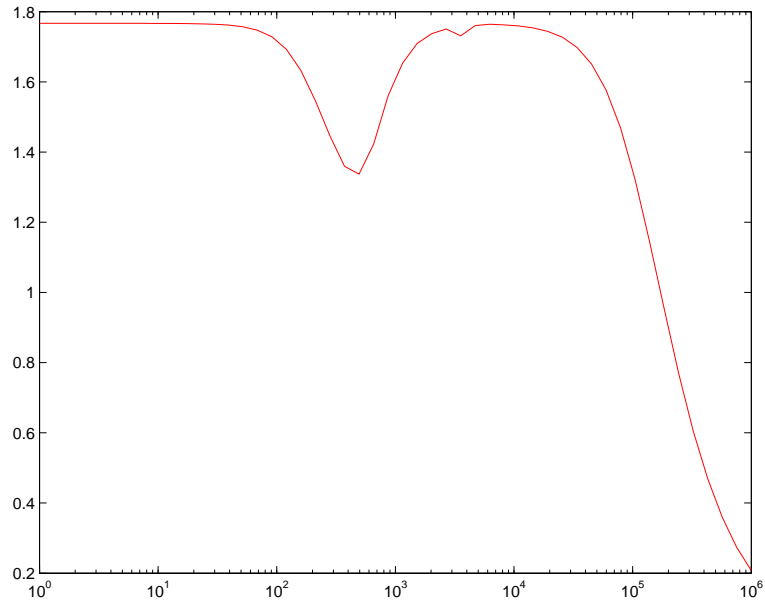


Figure 39: Nominal performance of the closed loop system for K_μ

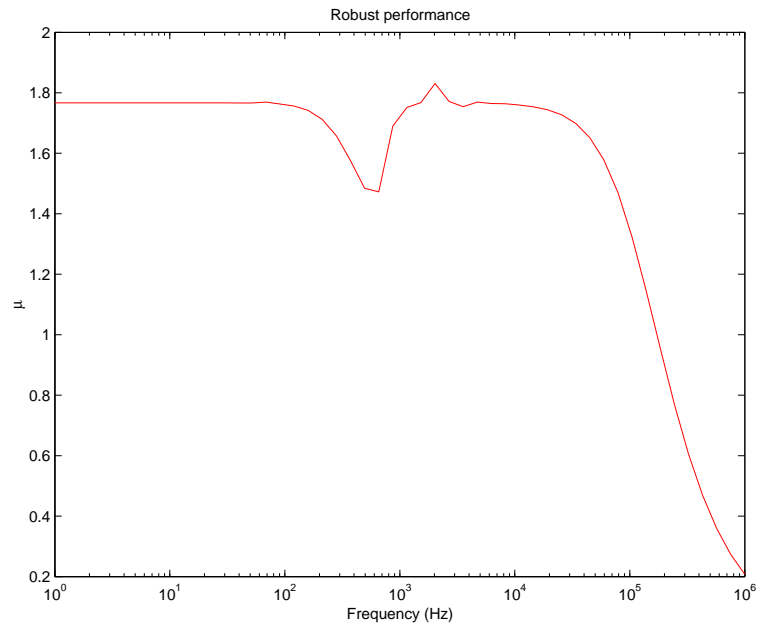


Figure 40: Robust performance of the closed loop system for K_μ

attenuation for low-frequencies is more than 560 times (55 dB). Hence low frequency disturbances will have very small effect on the closed-loop system output.

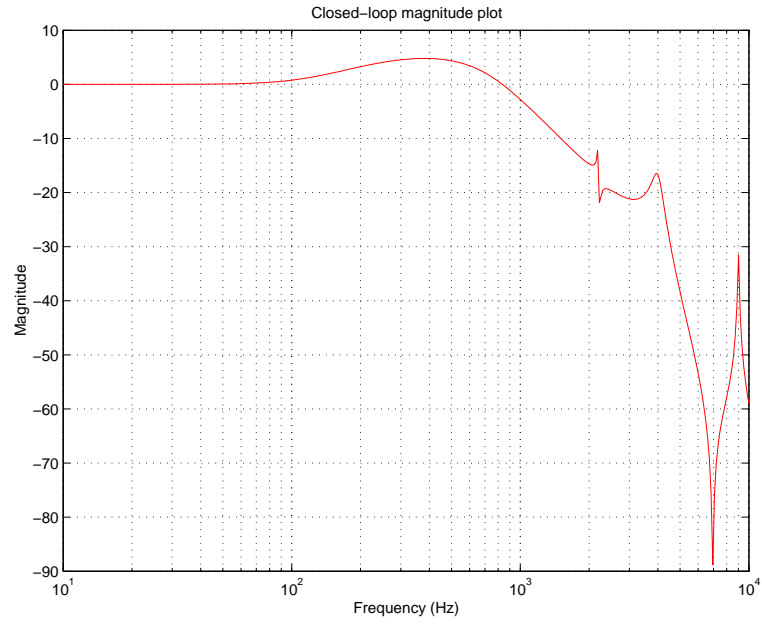


Figure 41: Magnitude plot of the closed-loop system for K_μ

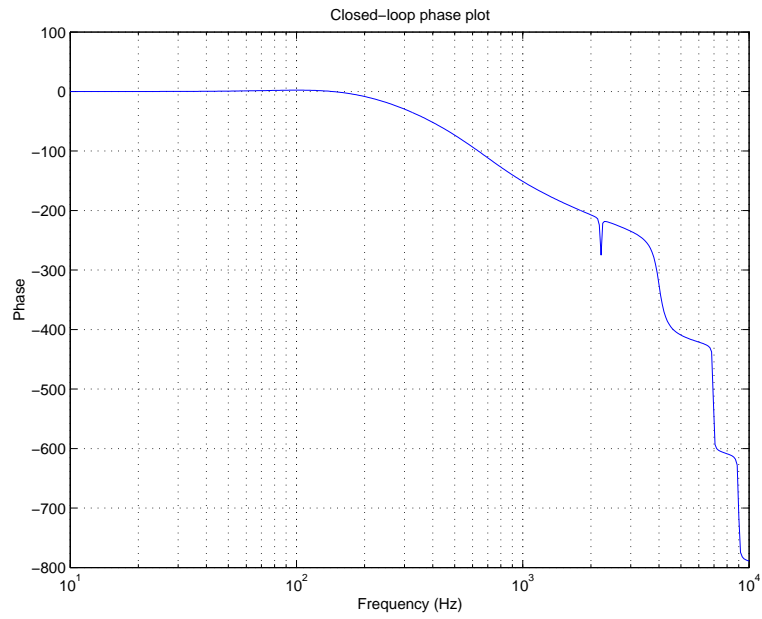


Figure 42: Phase plot of the closed-loop system for K_μ

In this way the computed μ controller ensures both robust stability and performance and disturbance attenuation.

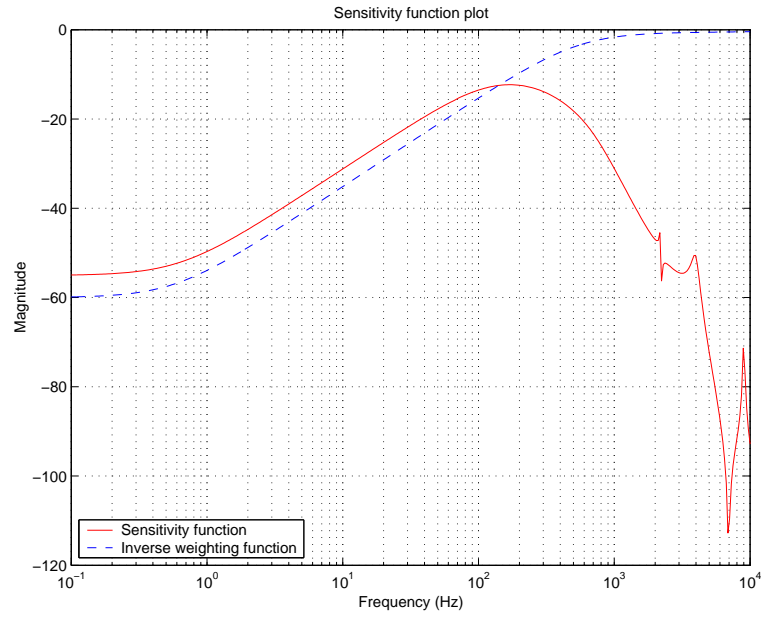


Figure 43: Sensitivity function plot for K_μ

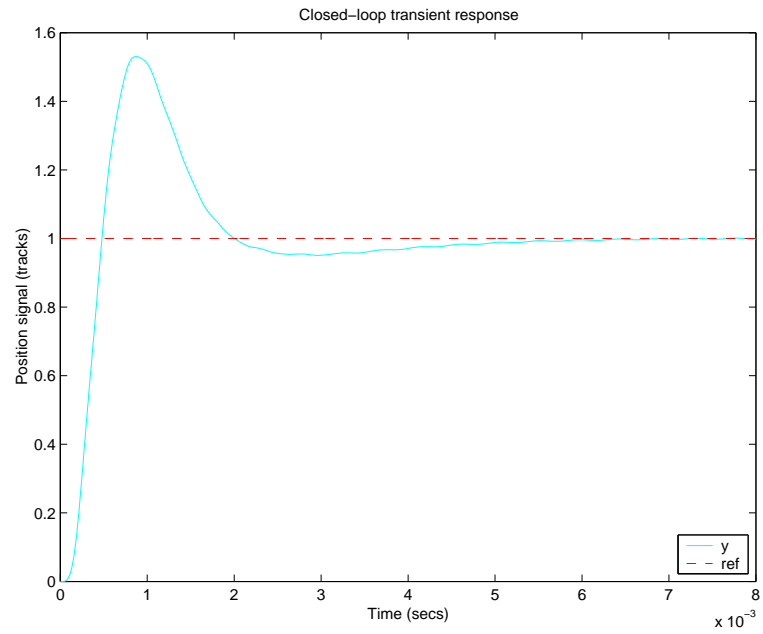


Figure 44: Transient response of the closed-loop system for K_μ

In Figure 44 we show the transient response of the system to a reference, equivalent to 1 track.

The overshoot is about 53% and the settling time is 1.8 *ms*, which shows that the system dynamics is satisfactory.

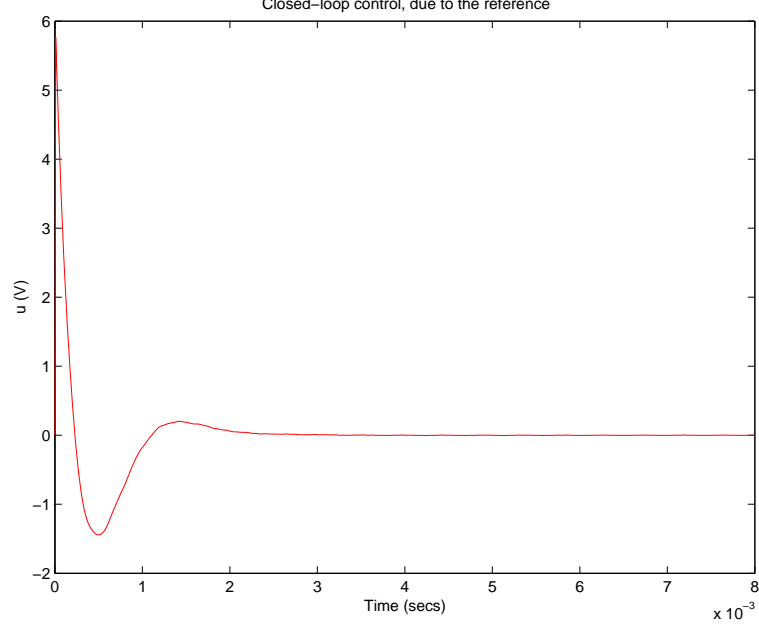


Figure 45: Control action for K_μ

The maximum of control action (Figure 45) is 5.76 V, which is the greatest one in comparison with the rest controllers.

In Figure 46 we show the transient response due to a step disturbance of 1 N. The dynamic error is less than 7.2% from the track width and the steady state error is practically equal to zero.

8 Comparison of the systems with three controllers

In Figure 47 we compare the frequency responses of the structured singular values obtained in the robust stability analysis of the systems with three controllers (\mathcal{H}_∞ , LSHD and μ). The three responses are very close. The best robustness is achieved by using the μ controller.

The comparison of the nominal performance for the three controllers, done in Figure 48, shows that the performance in case of LSHD controller for low frequencies is much worse than in the case of \mathcal{H}_∞ and μ controllers. This is due to the fact that the performance specifications used in the \mathcal{H}_∞ design and μ design are not used in the design of the LSHD controller.

The robust performance for the three controllers is shown in Figure 49. The best performance

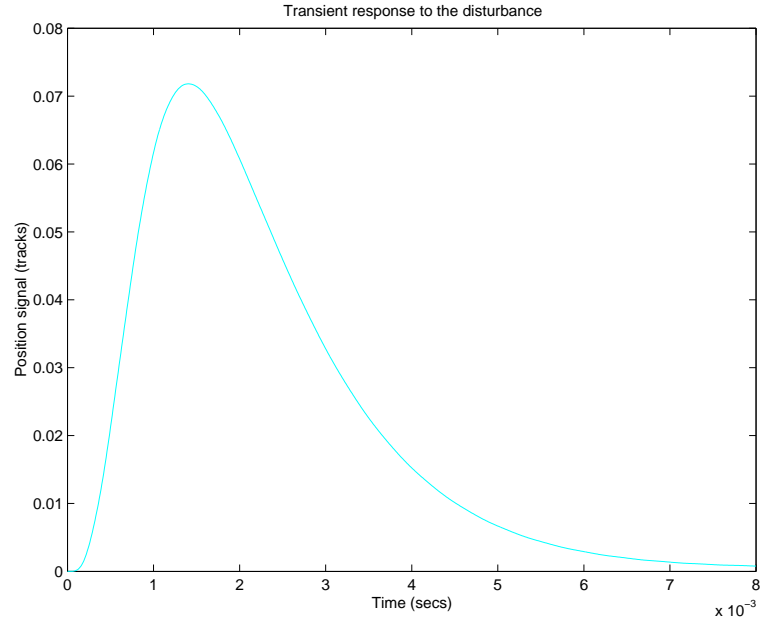


Figure 46: Disturbance response of the closed-loop system for K_μ

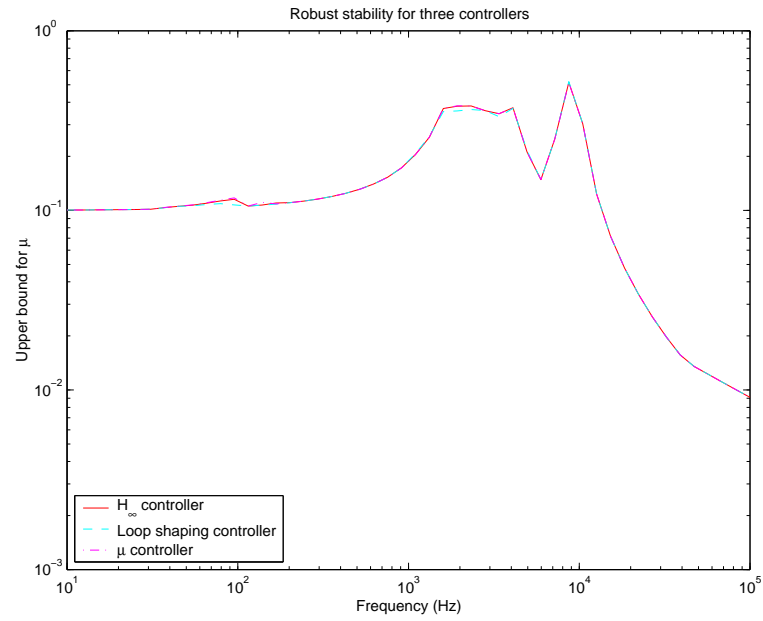


Figure 47: Robust stability of the closed-loop system

has the system with \mathcal{H}_∞ controller.

The robust stability and robust performance analysis shows that worse results in respect to

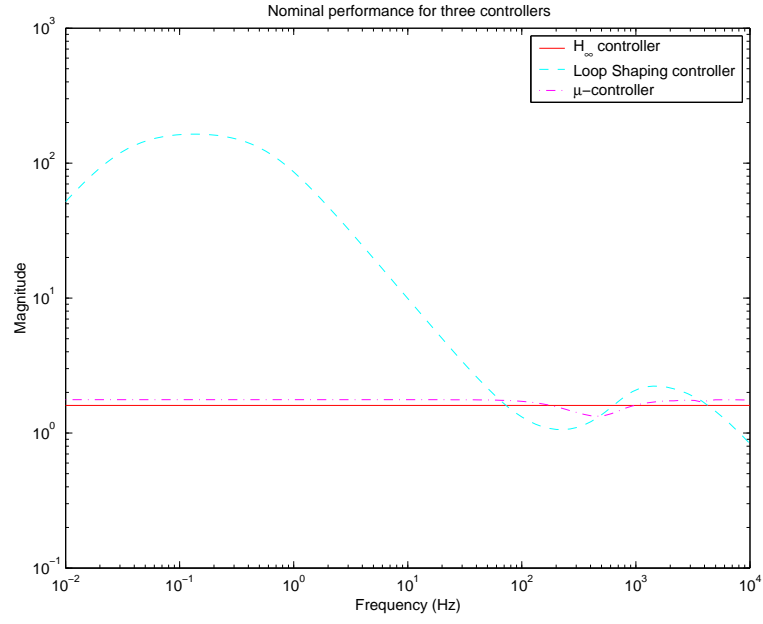


Figure 48: Nominal performance of the closed-loop system

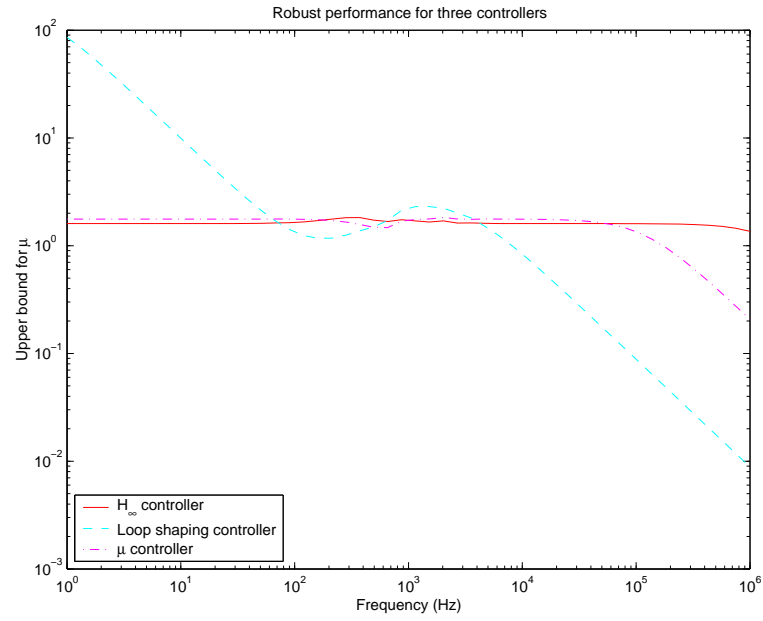


Figure 49: Robust performance of the closed-loop system

the corresponding property are obtained for the resonance frequency of 2.2 kHz .

The Bode plots of the closed-loop systems with the three controllers are shown in Figures 50

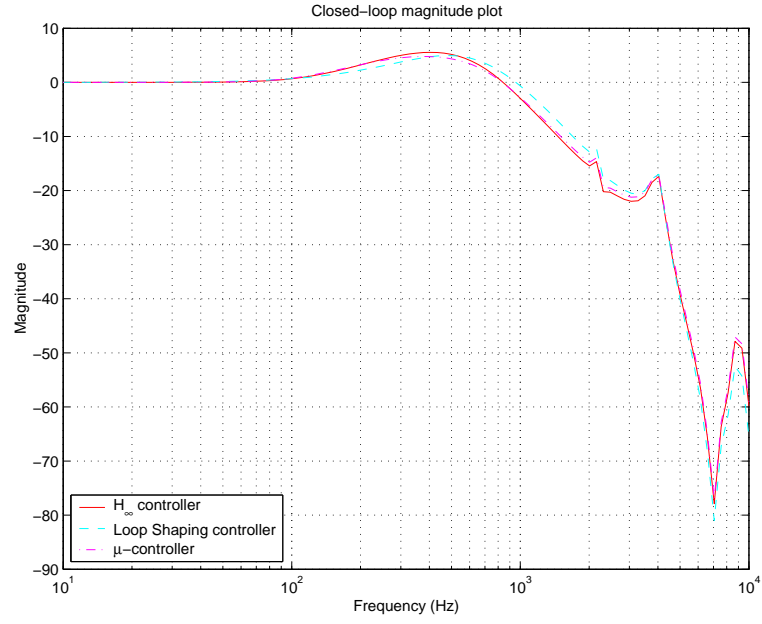


Figure 50: Magnitude plots of the closed-loop systems

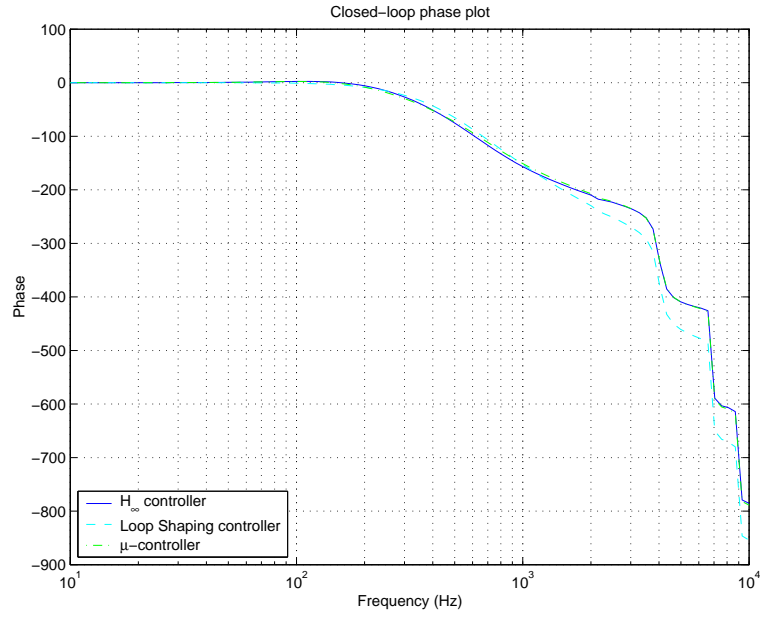


Figure 51: Phase plots of the closed-loop systems

and 51. It is seen that the system with LSHD controller has the largest bandwidth which leads to a fastest transient response. A larger bandwidth, however, may also lead to larger effect of the

noises.

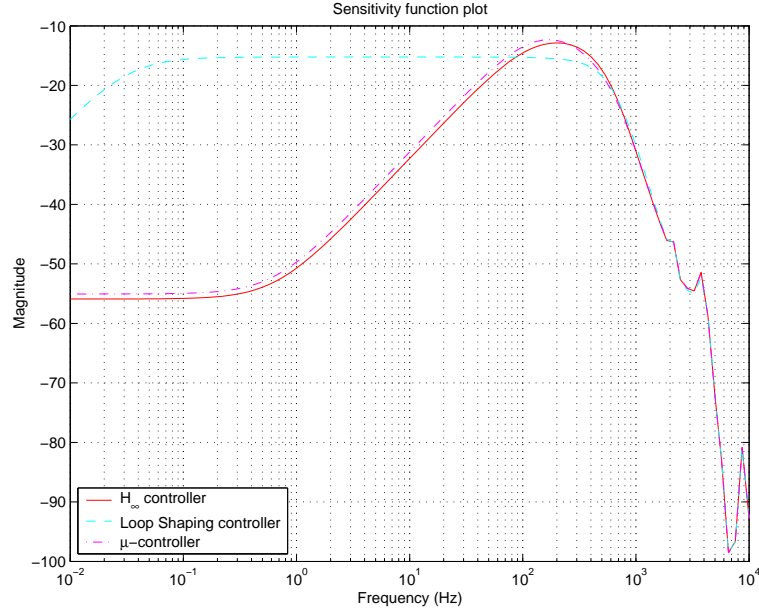


Figure 52: Sensitivity function plots

The sensitivity function plots of the system (Figure 52) show that the influence of the disturbance on the system output is largest in the case of LSHD controller. The value of the sensitivity function for this controller is -15 dB in the range from 0.1 Hz to 100 Hz which means that the disturbances in this range will not be sufficiently attenuated. Better disturbance attenuation can be achieved by choosing higher gain in the pre-filter. This may lead, however, to greater overshoot of the transient response.

The Bode plots of the three controllers are compared in Figures 53 and 54. It is seen that the LSHD controller has a very low gain in the range from 0.1 Hz to 100 Hz which is the reason for the weak attenuation of the disturbances in this range.

The comparison of the robust stability and robust performance for the three controllers, as well as the comparison of the corresponding transient responses shows that it is reasonable to prefer the μ controller.

9 Order reduction of the μ -controller

As mentioned above, the controller obtained by the μ -synthesis is initially of 38-th order. It is useful to reduce as much as possible the controller order which will simplify the implementation.

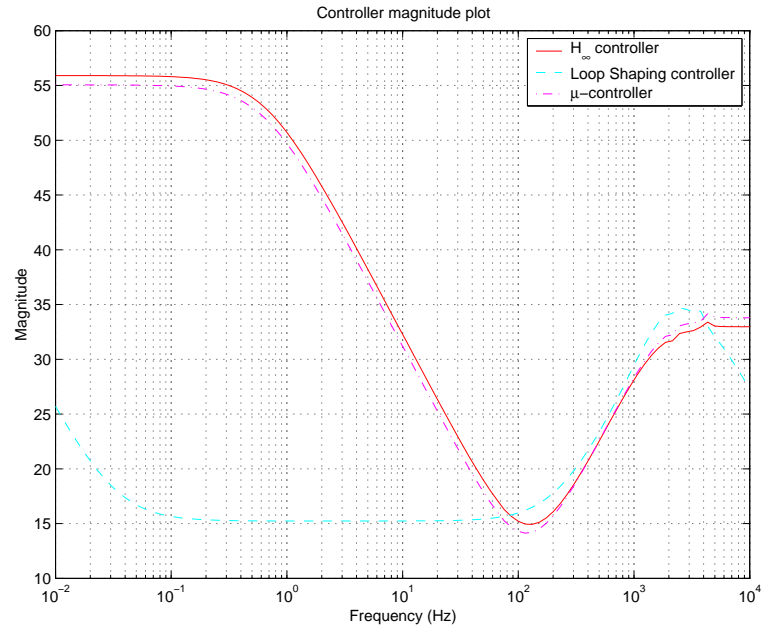


Figure 53: Magnitude plots of the controllers

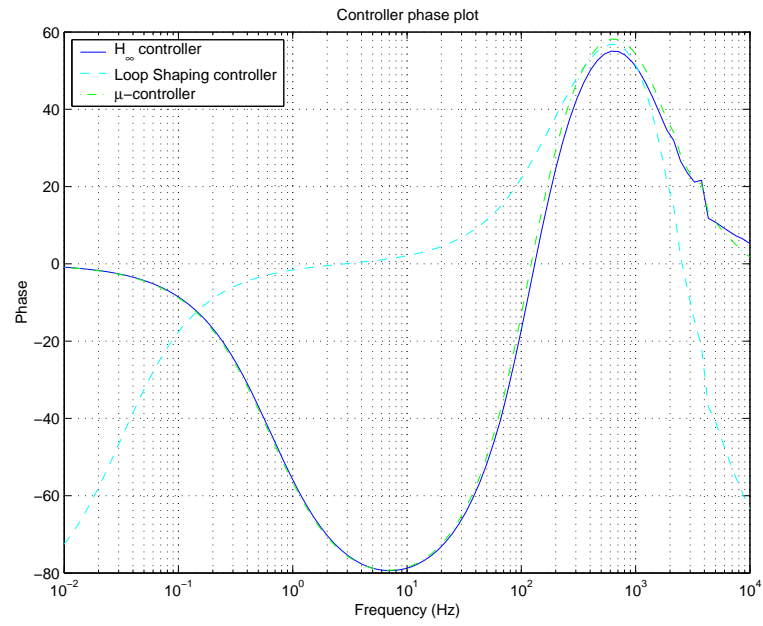


Figure 54: Phase plots of the controllers

To do this we use system balancing followed by optimal Hankel approximation which allows to

reduce the controller order to 11. Further reduction of the controller order leads to deterioration of the closed-loop transient responses.

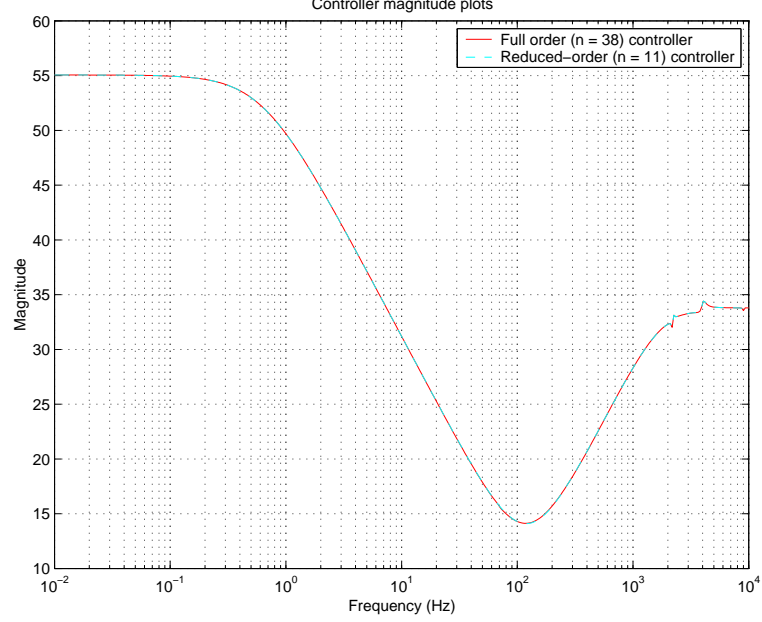


Figure 55: Magnitude plots of the full order and reduced order controllers

In Figures 55 and 56 we compare the Bode plots of the full order and reduced order controllers. The plots are very closed which implies similar performance in the closed-loop system. In particular, the transient responses of the closed-loop system with full order or with the reduced order controller are practically undistinguishable.

10 Simulation of the nonlinear servo system

In order to obtain a realistic impression about the system behaviour, the closed-loop nonlinear servo system with μ controller is simulated by using SIMULINK². For this aim the controller is discretized with sampling period $T = 2 \times 10^{-5} s$ which ensures dynamics closed to the dynamics of the continuous-time system. In the simulation we take into account the amplifier saturation and the back emf generated in the voice coil, which were neglected in the investigation of the linearized system.

The block diagram of the SIMULINK-model is shown in Figure 57. This model involves

²SIMULINK is a trade mark of The Mathworks, Inc.

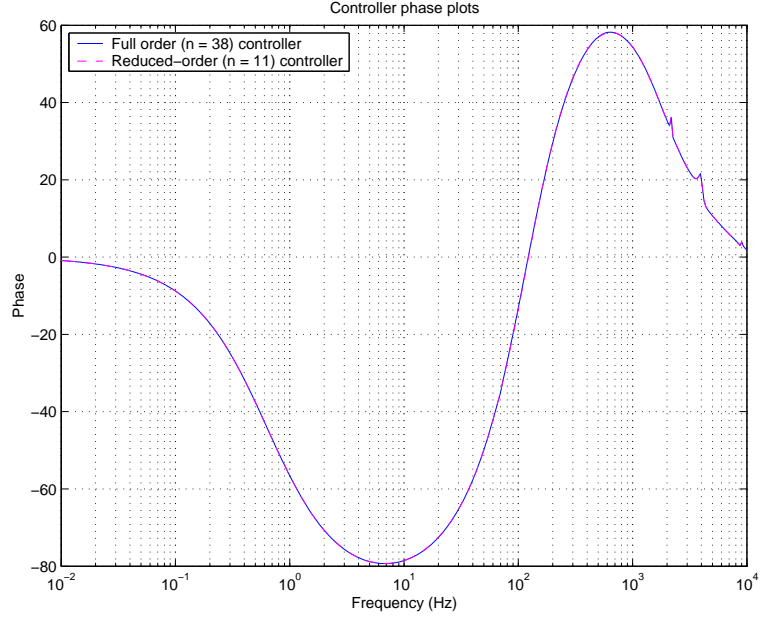


Figure 56: Phase plots of the full order and reduced order controllers

the discrete controller of 11-th order, power amplifier with voice coil, parallel connection of four resonance modes and rigid body dynamics which accounts for the viscous friction. The analog-to-digital converter is 16-bit with maximum input voltage 2.5 V and the digital-to-analog converter is also 16-bit with maximum output voltage 10 V . It is supposed that the discrete controller is realised on a Digital Signal Processor (DSP) with sufficiently large word length (64 bits).

In Figure 58 we show the transient response and in Figure 59 - the disturbance response of the nonlinear system for sampling frequency equal to 50 KHz . The overshoot is 44% and the settling time is less than 1.82 ms . The decreasing of the overshoot in comparison with the process shown in Figure 44, is due to the effect of the back emf generated in the voice coil as well as to the saturation of the amplifier.

In Figure 60 we show the control action for a reference equivalent to one track and in Figure 61 - the output of the power amplifier. It is seen that at the beginning of the response the output voltage of the amplifier is 34 V , i.e. the amplifier saturates. The saturation appear for a relatively small control signal due to the back emf in the voice coil.

The transient responses obtained in the nonlinear system show that controller designed ensures satisfactory dynamics of the closed-loop system.

The controller designed is appropriate for small reference signals (equivalent to several tracks).

SIMULINK model of the nonlinear sample-data Disk Drive Servo System

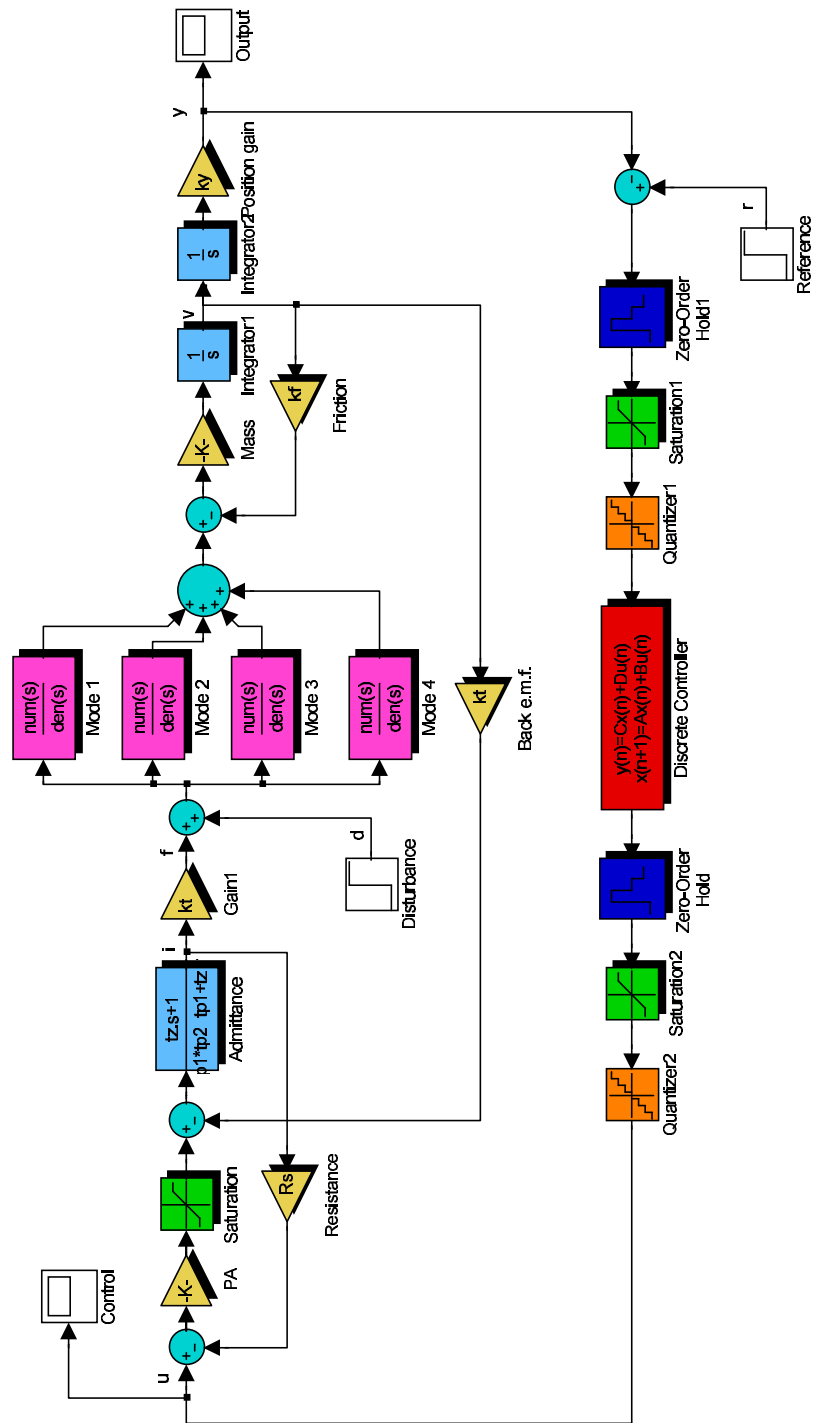


Figure 57: SIMULINK-model of the nonlinear sampled data system

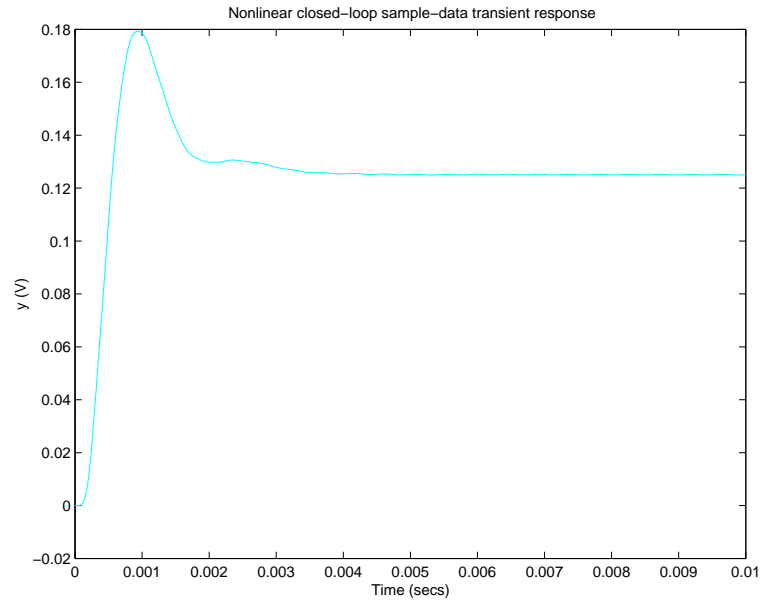


Figure 58: Transient response of the nonlinear sampled-data system

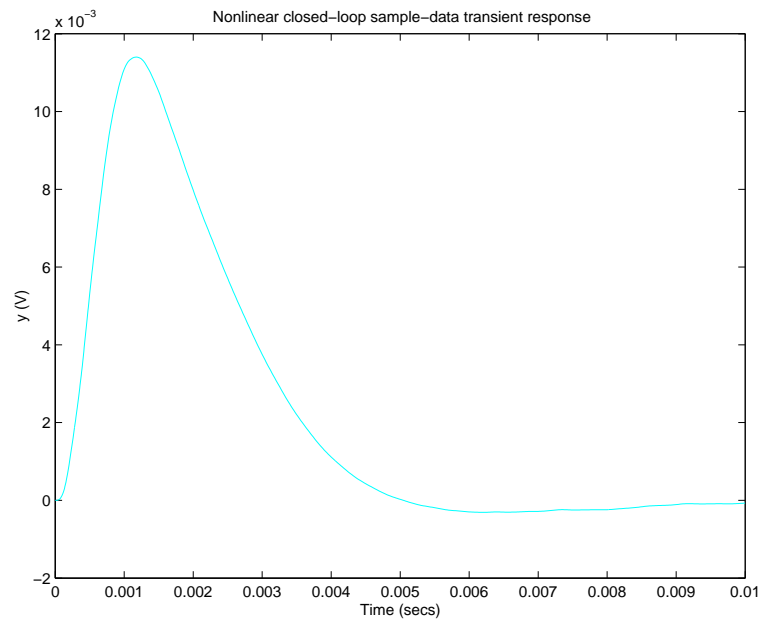


Figure 59: Disturbance response of the nonlinear sampled-data system

For larger references the amplifier saturates and it is necessary to implement time-optimal controller.

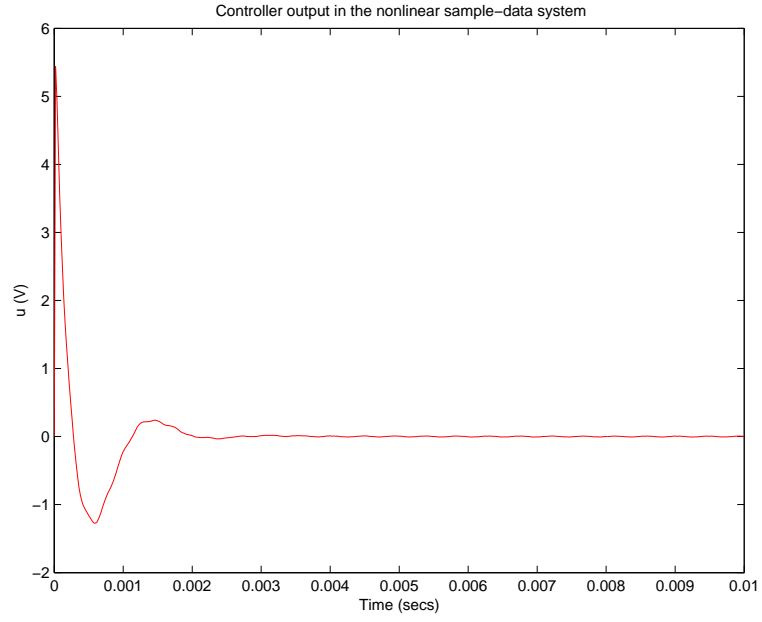


Figure 60: Control action in the nonlinear sampled-data system

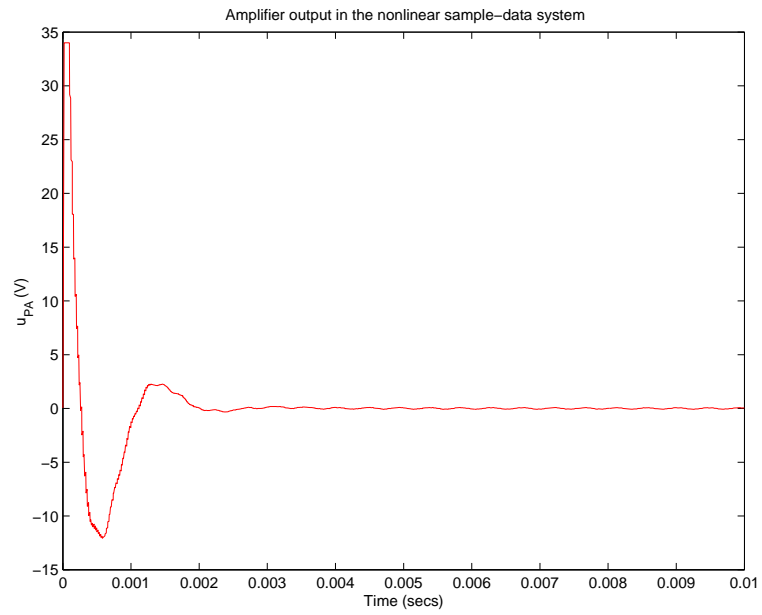


Figure 61: Amplifier output in the nonlinear sampled-data system

11 Conclusions

In this paper, the design of three robust controllers for a Disk Drive Servo System using \mathcal{H}_∞ -synthesis, Loop Shaping Design and μ -synthesis techniques was presented. The comparison of

system performance for the three controllers makes possible to derive the following conclusions:

1. The implementation of all three controllers gives satisfactory results in respect to the robustness and performance. All three controllers ensure robust stability of the closed-loop system. The best robust performance is achieved by using the \mathcal{H}_∞ controller but in this case the overshoot and the settling time are very large. The closed-loop system with μ controller has slightly worse robust performance but its transient response is better. The implementation of the LSHD controller gives the best results in respect to the overshoot and settling time. Also, the corresponding design is the easiest one since it is not necessary to look for optimal weighting functions. This controller, however, leads to the worst performance in the low frequency range. In the given case the best tradeoff between the robustness and transient response requirements is achieved by using the μ controller which is due, to some extent, to the specially chosen weighting functions.
2. The number of the original uncertain parameters is very large (more than 25 in the given case). This complicates the derivation of the uncertainty model and requires a lot of computations. That is why it is necessary to investigate the parameter importance in respect to the robustness and performance in order to reduce their number to acceptable value (say, 10-20).
3. Even for reduced number of uncertain parameters it is possible that the μ -synthesis can not be performed due to the very large value of γ in the \mathcal{H}_∞ step of the D-K iteration. In such cases the design is done taking into account only some of the uncertainties and after that a robust stability analysis is performed taking into account all uncertainties.
4. The controller order is highest in the case of μ -synthesis and depends on the plant order, the order of the weighting functions and the order of the diagonal elements approximations. Even for low order systems the controller can be of high order which complicates its implementation. That is why the controller design should be followed by order reduction. In practice the controllers used are of order between 8 and 15. It is mentioned in the literature [4], that the implementation of controllers of order up to 20 can be done with approximation errors less than 0.002 dB.

In the design, the \mathcal{H}_∞ controller and LSHD controller were computed by using the SLICOT mex-files `conhin` and `clsdp`. The structured singular value μ , necessary in the robust stability and robust performance analysis, as well as in the μ design, was calculated using the SLICOT mex-file `mucomp`. The computation experience shows that the SLICOT routines may perform better than the counterpart routines in MATLAB in terms of speed and accuracy.

References

- [1] P. Benner, V. Mehrmann, V. Sima, S. Van Huffel, and A. Varga. SLICOT - A subroutine library in systems and control theory. *Applied and Computational Control, Signals, and Circuits*, **1**, chapter 10:499-539, 1999.
- [2] G.F. Franklin, J.D. Powell and M.L. Workman. *Digital Control of Dynamic Systems*, 3rd ed. Addison-Wesley Pub. Co., 1998.
- [3] G.J. Balas, J.C. Doyle, K. Glover, A. Packard and R. Smith. *μ -Analysis and Synthesis Toolbox User's Guide*. The MathWorks Inc., Natick, MA, 1998.
- [4] B.J. Lurie and P.J. Enright. *Classical Feedback Control with MATLAB*. Marcel Dekker, NY, 2000.
- [5] D.C. MacFarlane and K. Glover. *Robust Controller Design Using Normalized Coprime Factor Plant Descriptions*. Lecture Notes in Control and Information Sciences, **vol.136**. Springer-Verlag, Berlin, 1990.
- [6] K. Zhou, J.C. Doyle and K. Glover. *Robust and Optimal Control*. Prentice-Hall, Upper Saddle River, NJ, 1996.
- [7] P.Hr. Petkov, D.-W. Gu and M.M. Konstantinov. *Fortran 77 Routines for \mathcal{H}_∞ and \mathcal{H}_2 Design of Continuous-Time Linear Control Systems*. **NICONET** Report 1998-8, <http://www.win.tue.nl/wgs/niconet.html>, 1998.
- [8] D.-W. Gu, P.Hr. Petkov and M.M. Konstantinov. *An Introduction to \mathcal{H}_∞ Optimisation Designs*. **NICONET** Report 1999-4, <http://www.win.tue.nl/wgs/niconet.html>, 1999.
- [9] D.-W. Gu, P.Hr. Petkov and M.M. Konstantinov. *\mathcal{H}_∞ Loop Shaping Design Procedure Routines in SLICOT*. **NICONET** Report 1999-15, <http://www.win.tue.nl/wgs/niconet.html>, 1999.